Mon. Not. R. astr. Soc. (1990) **247**, 19–42

The redshift cut-off in the luminosity function of radio galaxies and quasars

J. S. Dunlop
Department of Astronomy, University of Edinburgh, Blackford Hill, Edinburgh EH9 3HJ and *School of Physics and Astronomy, Lancashire Polytechnic, Preston PR1 2TQ*

J. A. Peacock
Royal Observatory, Blackford Hill, Edinburgh EH9 3HJ

Accepted 1990 May 14. Received 1990 May 10; in original form 1989 December 13

SUMMARY

We describe a new investigation of the evolution of the radio luminosity function for extragalactic radio sources, with particular emphasis on the behaviour at high redshifts. Our analysis contrasts free-form and simple parametric modelling with model-independent techniques. Using data from a new complete sample at 2.7 GHz (the $S > 100$ mJy Parkes selected regions) in addition to previously studied data sets, we are able to reach several important conclusions, as follows.

(i) We strengthen previous conclusions that a 'redshift cut-off' exists in the distribution of flat-spectrum quasars, in the sense of a reduction in comoving density by a factor of $\simeq 5$ over the redshift range 2–4.

(ii) We present the first clear evidence that similar behaviour also appears to apply to steep-spectrum quasars *and* radio galaxies, making this decline a universal feature for all high-luminosity radio sources. However, the 'cut-off' does appear to be more abrupt for the flat-spectrum population. These statements still depend on the accuracy of our redshift estimates for faint galaxies, and we identify future observations which can remove the remaining uncertainty.

(iii) By allowing for a slowly evolving population at low luminosities, we are able to fit all existing redshift and source-count data with a model whereby luminous sources undergo pure luminosity evolution (but this is only possible for $\Omega_0 \simeq 1$). We have also successfully constructed a luminosity/density evolution model, with continuing positive luminosity evolution plus a depression in comoving density at high redshift. Further improvements in the database are required to distinguish between these two alternative forms of high-redshift evolution.

1 INTRODUCTION

The question of how the population of active galaxies evolves at high redshift has been an area of considerable interest for most of the last two decades. The term 'redshift cut-off' entered the literature in a paper by Sandage (1972), which considered the redshifts of quasar identifications in the 3C, 4C and Parkes catalogues. At that time, the highest redshift known was $z = 2.8$, and Sandage conjectured that no more distant objects might exist. However, within a year the discovery of OQ172 at $z = 3.53$ (Wampler *et al.* 1973) distracted attention away from redshifts in the region 2–3. In retrospect this was unfortunate, as quasar research then became something of a competition to break the redshift record. Several years were needed following this to understand the selection effects which applied to the various optical search methods (e.g. Smith 1986). The first author who was able to establish something important from an *unsuccessful* search for high-redshift objects was probably Osmer (1982), who concluded on the basis of a 4-m grism search that optically selected quasars at $z \simeq 4$ have a reduced comoving density. However, confirmation of this result has been delayed by the problem of achieving genuine completeness in optically selected samples; only relatively recently have other groups been able to report preliminary results consistent with Osmer's, based on multicolour and Grism selection (Warren, Hewett & Osmer 1988; Schmidt, Schneider & Gunn 1988). Radio selection provides better prospects of an unambiguous result, but the original area of interest pointed out by Sandage remained little studied for

some years. For radio galaxies of extremely low luminosity, a reduction in comoving density at $z \gtrsim 1$ was claimed by Windhorst (1984); this luminosity regime is discussed in Section 4.4.2. At high luminosities, Peacock (1985) performed a statistical analysis of the redshift data in complete samples of radio galaxies and quasars. The conclusion of that work was that evidence existed for a reduction in the comoving density of radio-loud quasars of the compact flat-spectrum class ($\alpha < 0.5$, where $S \propto \nu^{-\alpha}$) beyond a redshift of about 2. However, at that time the data on steep-spectrum radio quasars and also on the much larger population of radio galaxies were too sparse for it to be possible to say whether similar behaviour applied for them also. Since then, we have worked as part of a collaboration which aimed to provide optical data on a radio sample which is fainter than those available in 1985: the Parkes selected regions (Downes *et al.* 1986; Dunlop *et al.* 1989a). The main concern of the present study is therefore to investigate what light this new database (and other recent results) can shed on the issue of the redshift cut-off for steep-spectrum sources.

The layout of the paper is as follows. Section 2 describes the areas in which the database used by Peacock (1985) has since been improved and extended. Particular attention is paid to the method of redshift estimation used for the faintest galaxies in the selected regions sample, because these data play such a crucial role in determining the form of the radio luminosity function (RLF) at high redshift. In the first part of Section 3 the free-form modelling technique of Peacock & Gull (1981) and Peacock (1985) is applied to the new database to investigate the range of evolving RLFs allowed by the data. The opposite approach is then adopted and two simple parametric models of physical interest (pure luminosity evolution and luminosity/density evolution) are attempted. The evidence for a high-redshift cut-off indicated by this modelling work is investigated in a more direct manner in Section 4; a simple 2-parameter model of the high-redshift RLF is considered, and model-independent evidence for the redshift cutoff is tested via a variant of the $V/V_{\max}$ statistic. Section 4 closes with some predictions for the expected number of high-redshift objects in existing radio samples, and anticipates how future improvements in data will impact on our knowledge of high-redshift evolution. Finally, our main conclusions are summarized and discussed in Section 5.

Throughout, we adopt a Hubble constant of $H_0 = 50$ km s^{-1} Mpc^{-1}; for other values, luminosities scale as H_0^{-2} and densities as H_0^3. Note that the units of the luminosity function are sources per comoving Mpc^3 per unit interval of $\log_{10} P$.

2 NEW DATA

The most significant addition to the data used by Peacock (1985) is the Parkes selected regions database; this provides a vital extension of the complete S–z data to low flux densities, and is discussed in more detail below.

Most of the additional, less-detailed data used to constrain the RLF have undergone relatively little modification. This information consisted of estimates of the local RLF, source counts between 408 MHz and 5 GHz, and approximate redshift distributions estimated from the identification content of various faint radio samples. However, since 1985, several new relevant sets of data have been published; we now discuss these, along with some inconsistencies in previous data which have thereby been exposed.

2.1 The local radio luminosity function

In recent years there have been several new determinations of the local radio luminosity function. Both the steep- and flat-spectrum local RLFs have therefore been re-evaluated using the data from Toffolatti *et al.* (1987) and Subrahmanya & Harnett (1987), which provided two new independent determinations of the steep-spectrum local RLF at 2.7 GHz, and one new determination of the flat-spectrum local RLF. These new data were incorporated into the database along with the existing local RLF data used by Peacock (1985), which have now been corrected for the counting error in the data of Cameron (1971) pointed out by Toffolatti *et al.* (1987). The updated local RLF data are given in Table 1 and illustrated in Fig. 1. For the translation to 2.7 GHz, a spectral index of 0.8 has been assumed, as discussed in Section 3.2. These determinations are in good qualitative agreement, but there are some regions of statistical disagreement in the steep-spectrum data (particularly around $P_{2.7} \simeq 10^{21}$ W Hz^{-1} sr^{-1}, despite the above corrections to Cameron's data). These flat residual symmetric errors, probably due to correction from different selected frequencies and incompletenesses. To represent these an error of 0.2 in $\log_{10}(\rho)$ has been added in quadrature to the formal errors given in Table 1; a single polynomial is then consistent with all three sets of data.

Peacock (1985) constrained his model RLFs to be consistent with the local RLF out to $z = 0.2$. However, with the improved accuracy of the new local RLF determination, it was found necessary to relax the formal errors by a further 0.2 [in $\log_{10}(\rho)$] at $z = 0.2$ in order to achieve acceptable model fits. This is not unreasonable, since studies which indicate no evolution out to $z = 0.2$ have errors on ρ of this order (Windhorst 1984).

2.2 Source counts

Several improvements in the source-count data have taken place since 1985. At bright flux densities, the large-area 5-GHz MG survey (Bennett, Lawrence & Burke 1985) has greatly improved the statistics on the total counts down to ~ 10 mJy. At the opposite extreme, counts at 1.4 and 5 GHz have now been extended down to ~ 50 μJy. These improvements are chronicled by Kellermann & Wall (1987). Attempts to incorporate these new data into the RLF modelling revealed at any early stage, however, that there appear to be some inconsistencies in the count data, which we now discuss.

The problem can be best illustrated by plotting the source counts from various frequencies directly on top of one another. The wide range of spectral indices prevents a simple scaling of the total counts being possible, but the steep-spectrum counts alone may be treated in this way. Where spectrally separated counts are not available (at 408 MHz or at faint flux densities), the flat-spectrum contribution is usually small and can be subtracted off to adequate accuracy by using a model: $dn_{\rm flat}/dS = 45(S/{\rm Jy})^{-2.5} \exp[-\ln^2(S/{\rm Jy})/8]$ sr^{-1} was adopted. Fig. 2 thus gives a composite plot of steep-spectrum counts at 2.7 GHz, scaled using $\alpha = 0.85$. The

Table 1. The local RLF at 2.7 GHz.

a) Steep-spectrum

Determination 1 (modified from Peacock 1985)		Determination 2 (Toffolatti *et al.* 1987)		Determination 3 (Subrahmanya & Harnett 1987)	
$\log_{10}(P_{2.7})$	$\log_{10}(\rho)$	$\log_{10}(P_{2.7})$	$\log_{10}(\rho)$	$\log_{10}(P_{2.7})$	$\log_{10}(\rho)$
18.27	-1.11 ± 0.85	19.34	-2.00 ± 0.73	18.50	-2.05 ± 0.31
18.67	-0.46 ± 0.85	20.09	-2.80 ± 0.07	18.90	-2.42 ± 0.25
19.07	-1.46 ± 0.85	20.59	-3.06 ± 0.09	19.30	-2.57 ± 0.31
19.47	-1.56 ± 0.85	21.09	-3.45 ± 0.05	19.70	-2.53 ± 0.11
19.67	-1.71 ± 0.85	21.59	-4.14 ± 0.05	20.10	-2.76 ± 0.10
19.87	-2.11 ± 0.85	22.09	-4.67 ± 0.09	20.50	-2.70 ± 0.08
20.07	-2.30 ± 0.85	22.59	-5.28 ± 0.10	20.90	-2.93 ± 0.08
20.35	-2.60 ± 0.11	23.09	-5.50 ± 0.08	21.30	-3.58 ± 0.13
20.75	-2.57 ± 0.08	23.59	-5.82 ± 0.08	21.70	-4.43 ± 0.26
21.15	-2.91 ± 0.08	24.09	-6.18 ± 0.07	22.10	-5.53 ± 0.25
21.55	-4.07 ± 0.22	24.59	-6.96 ± 0.10		
21.95	-4.45 ± 0.31	25.09	-7.43 ± 0.22		
22.75	-5.51 ± 0.25				
23.25	-5.92 ± 0.11				
23.75	-6.06 ± 0.11				
24.25	-6.74 ± 0.15				
24.65	-7.01 ± 0.18				
25.05	-7.35 ± 0.31				

b) Flat-spectrum

Determination 1 (Peacock 1985)		Determination 2 (Toffolatti *et al.* 1987)	
$\log_{10}(P_{2.7})$	$\log_{10}(\rho)$	$\log_{10}(P_{2.7})$	$\log_{10}(\rho)$
19.40	-3.10 ± 0.31	20.00	-4.10 ± 0.43
20.90	-4.12 ± 0.22	20.75	-4.46 ± 0.31
22.10	-5.48 ± 0.31	21.25	-4.82 ± 0.19
22.85	-5.83 ± 0.18	21.75	-5.26 ± 0.19
23.60	-6.73 ± 0.31	22.25	-5.46 ± 0.22
		22.75	-6.06 ± 0.31
		23.25	-6.90 ± 0.22
		23.75	-7.38 ± 0.43
		24.25	-7.05 ± 0.19

appearance of the plot depends little on α within reasonable limits; the agreement of the various data sets is generally excellent within the errors (and could be improved still further if we wished to account for known weak correlations of α with flux density). However, there are two rather obvious inconsistencies in the data at around 100 mJy and 100 μJy. At the faint end, the 5-GHz counts appear low by a factor of ~ 3 by comparison with the data at 1.4-GHz (consistency would require scaling with a spectral index of 1.6, which seems implausible). The fault appears likely to lie with the 5-GHz data as the 1.4-GHz points around 200 μJy come from VLA and Westerbork data, and these are in good agreement. The faintest three points in the 5-GHz data were thus ignored from the point of view of constraining the RLF.

More disturbing than this is the discrepancy around 100 mJy; the badly inconsistent point is the lowest bin of the Parkes 2.7-GHz counts (100–120 mJy), which comes from the selected regions. In this region, the 5GHz, 1.4-GHz and 408-MHz data are all in agreement that the steep-spectrum counts are $\Delta n/\Delta n_0 \simeq 0.7$, whereas the selected-region point gives a value of only 0.35 – implying an incompleteness in this region of a factor of 2. Such a discrepancy is too large to be attributed to errors in the spectral index assumptions. This is not really a new problem; examination of fig. 1 in Peacock (1985) shows that past model RLFs did not fit this data point very well. The discrepancy has come to light only now owing to the improved accuracy of the 5-GHz counts. One surprising aspect of this problem is that it is confined to the steep-spectrum population: there is no corresponding down-turn in the faintest bin of the 2.7-GHz flat-spectrum counts. Spectral mis-classification cannot be the problem, however, as this lowest flux-density bin contains 21 steep-spectrum sources but only 11 flat-spectrum; no more than 5 or so flat-spectrum sources could be transferred to the steep-spectrum bin without causing a problem with the flat-spectrum counts, and this is not enough to make up the deficit. In any case, there are no plausible candidates for mis-classification: the faintest flat-spectrum sources are all compact quasars. We are left with the hypothesis that there was incompleteness in the original survey. Appendix A shows that there is indeed evidence for this at at least the 20 per cent level between 100 and 120 mJy (but not at higher flux densities). Taking into account this internal evidence and the external comparison with other count data, we have adopted a scaling of total numbers in this bin of a factor of 1.5 (i.e. the effective area surveyed drops from 0.0753 to 0.05 sr). The most conservative procedure would of course be to drop the faintest sources altogether, but as there is no mechanism by which the incompleteness could contain a redshift bias, the *probability distribution* for the redshifts of these objects is still a useful cosmological datum.

2.3 The Condon–Ledden sample

Condon & Ledden (1982) reported optical identifications for a faint sample of flat-spectrum sources ($S > 15$ mJy at 5GHz), which was one of the data sets used by Peacock (1985). The fraction of the sample identified with galaxies to the Palomar Sky Survey limit was 46 per cent. This datum proved very hard to fit in the current revised modelling,

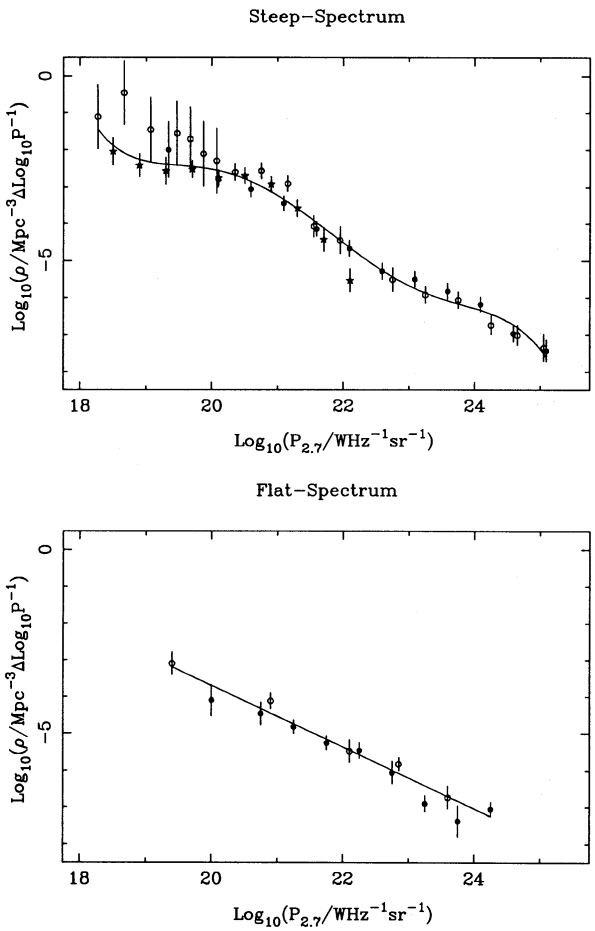

Figure 1. The local radio luminosity function at 2.7 GHz. The open circles are the (corrected) data used by Peacock (1985) (see references therein). The filled circles are the new determinations from the data of Toffolatti *et al.* (1987), while the stars are the new steep-spectrum local RLF determined from the data of Subrahmanya & Harnett (1987). The curves shown are best-fitting polynomials of order 1 and 5, respectively.

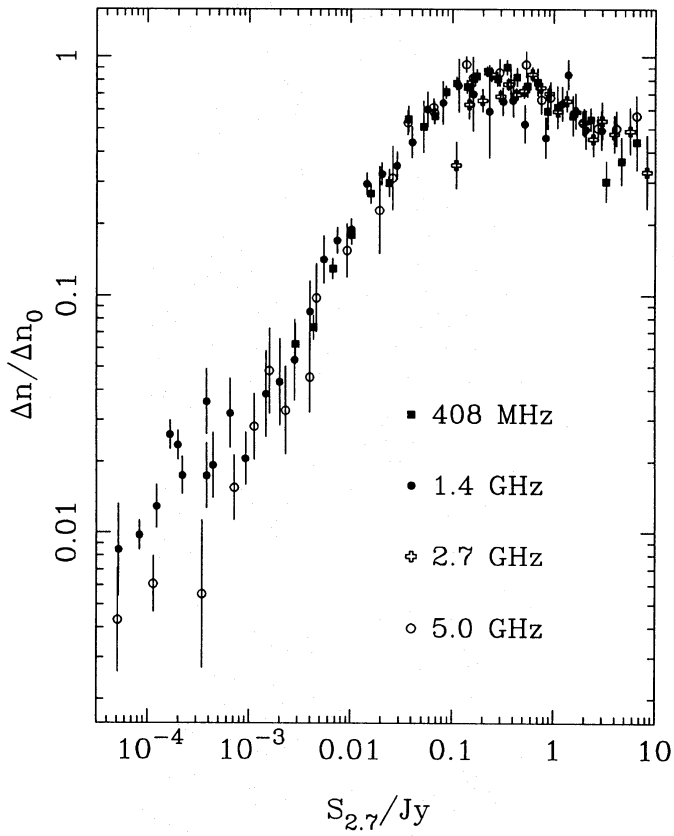

Figure 2. The steep-spectrum source counts at frequencies of 408 MHz, 1.4 GHz, 2.7 GHz and 5 GHz, scaled to 2.7 GHz assuming $\alpha = 0.85$. Spectrally separated counts are plotted where available, otherwise we show the total count minus a flat-spectrum contribution modelled as described in the text. The normalization is to the Euclidean count $N_0 = 100(S/\mathrm{Jy})^{-1.5}\ \mathrm{sr}^{-1}$.

prompting a re-examination of the sample; it seems likely that this figure is rather too high. Of the 17 galaxy identifications, six have $0.4 < \alpha < 0.5$, which suggests they may not be genuine flat-spectrum sources. Indeed, at least two of these are extended doubles. Removing these six objects from consideration leaves 11 galaxy identifications out of 40 flat-spectrum sources, or an assumed figure of 28 per cent of sources closer than the Palomar limit (assumed to correspond to $z = 0.6$). Model RLFs consistent with this revised figure could be found quite easily.

2.4 The 2.7-GHz complete sample database

The selected regions sample is important because it provides a low flux density extension (i.e. 0.1 Jy) to the existing complete sample database at 2.7 GHz. Previously the flux limits of the complete S–z data were 0.5 Jy for flat-spectrum sources and 1.5 Jy for steep-spectrum sources. The database at 2.7 GHz now consists of data taken from four complete samples:

(i) the $S_{2.7} > 0.1$ Jy Parkes selected regions sample;
(ii) the $S_{2.7} > 0.5$ Jy flat-spectrum sample selected by Peacock (1985) from the Parkes $\pm 4°$ zone (Wright *et al.* 1982);
(iii) the $S_{2.7} > 1.5$ Jy 'Northern-Sky' survey of Peacock & Wall (1981);
(iv) the $S_{2.7} > 2$ Jy 'All-Sky' survey of Wall & Peacock (1985).

Since these samples first appeared in print many new redshifts have been obtained. The revised versions of these four samples are given by Peacock, Prestage & Wall (in preparation), and their properties are summarized in Table 2.

To make maximum use of these data they must be combined into a single sample. After allowing for overlap between the surveys, the resulting combined data set consists of 524 sources (171 flat-spectrum and 353 steep-spectrum) of which only three sources remain unidentified and a further 4 per cent are identified but lack either a measured or securely estimated redshift (estimated from galaxy photometry – see below). The objects with uncertain redshifts are

Table 2. The complete-sample data at 2.7 GHz.

Sample	Area	No. of sources	No. of sources unidentified	No. of sources without z
$S_{2.7} > 0.1$ Jy	0.075 sr	178	0	96 (54%)
$S_{2.7} > 0.5$ Jy	0.584 sr	40	0	11 (28%)
$S_{2.7} > 1.5$ Jy	4.05 sr	171	0	21 (12%)
$S_{2.7} > 2.0$ Jy	9.81 sr	235	2	41 (17%)

either quasar candidates or objects for which the classification of the optical identification is uncertain.

2.5 Redshift estimation in the Parkes selected regions sample

There are two reasons why the problem of redshift estimation is particularly important in the selected regions sample. First, in this sample, estimated redshifts are required for a relatively large number of sources – Table 2 demonstrates that the spectroscopic content of the selected regions is low in comparison with that of the three brighter samples. Secondly, because it is the deepest of the four samples, the selected regions sample provides the strongest probe of high-redshift space – and so the redshift estimates for the fainter objects in this sample will strongly influence conclusions about the evolution and shape of the RLF at high z.

Redshift estimation is much more important in the study of the RLF for steep-spectrum sources than for those with flat spectra. Of the 35 new flat-spectrum sources provided by the selected regions in the flux-density range 0.5 Jy $> S_{2.7} >$ 0.1 Jy, 23 (66 per cent) have measured redshifts; this is because the bulk of the flat-spectrum identifications are quasars rather than galaxies. In contrast, of the 133 new steep-spectrum sources added to the database in the flux-density range 2 Jy $> S_{2.7} >$ 0.1 Jy, only 49 (37 per cent) have a measured redshift. In both the flat- and steep-spectrum samples the bulk of the objects without redshifts are galaxies rather than quasars. The problem of having to make a guess at the missing quasar redshifts is therefore not very serious in the present study (the method of redshift estimation for this small number of quasar candidates, and the adopted values are described in Dunlop *et al.* 1989a).

The crucial issue is therefore the estimation of redshifts for the faint galaxy identifications. For most of these objects K photometry had been obtained and so their redshifts could be estimated via the K–z relation for radio galaxies (which was investigated by Lilly & Longair 1984). Note that more K photometry is now available to us than was published in Dunlop *et al.* (1989a). At high z, infrared photometry provides the most accurate method of redshift estimation because, in contrast to the optical Hubble diagram, the K–z diagram is unaffected by the UV flux from small numbers of young stars. Lilly & Longair have demonstrated empirically that for the 3CR radio galaxies the dispersion in the K–z diagram does not increase significantly with z. For galaxies with K magnitudes in the range $13 < K \lesssim 18.5$, the empirical relation $\log_{10}(z) = -5.368 + 0.384\,K - 0.00385\,K^2$ was adopted for redshift estimation. This relation is given by Lilly, Longair & Allington-Smith (1985) as a good approximation to the K–z relation exhibited by the 3CR and 1-Jy radio galaxies. It is shown along with the most recent K–z data in Fig. 3 and is still clearly a very good description of the data. For the small number (8) of faint galaxies without K photometry, redshifts were estimated using the close relation between B–R and K (Dunlop *et al.* 1989a).

Since many rather important conclusions will flow from the redshift estimates we adopt, it is vital that the effects of varying assumptions are investigated. The first point to consider is the scatter about the K–z relation; Lilly & Longair (1984) estimated this to be about 0.4 mag (i.e. 20 per cent in redshift), independent of redshift. Such a scatter means that some of our very faint K detections could lie at redshifts significantly higher than we estimate from the mean K–z line. We have investigated this possibility: adding a random scatter of 20 per cent to the estimated redshifts produces a redshift distribution which is statistically indistinguishable from that which results when no scatter is assumed. It will therefore suffice to consider whether there may be systematic errors in our redshift estimates.

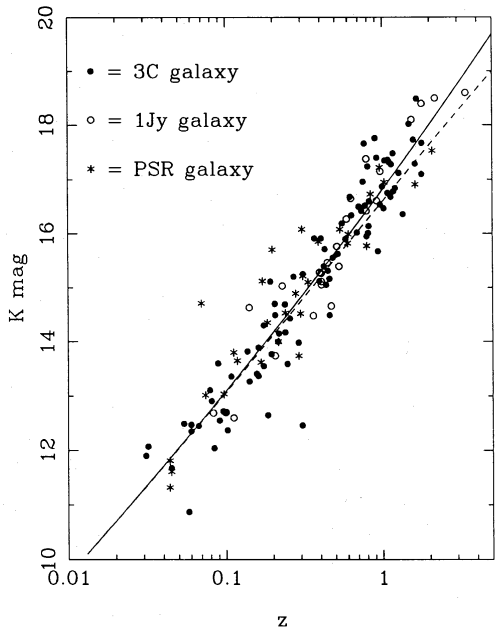

Figure 3. The K–z relations used to estimate the redshifts of faint galaxies in the selected regions. The curves represent feasible extrapolations of the Hubble relation beyond $K \simeq 17$, based on realistic models of galaxy evolution. The solid line is that used to make the MEAN-z redshift estimates, the dashed line is the HIGH-z modification. The solid circles are galaxies taken from the 3CR radio sample (Lilly & Longair 1984); the open circles are galaxies from the 1- Jy radio sample (Lilly *et al.* 1985); asterisks denote selected-region data.

There are two possibilities to consider: either systematic errors in our K photometry or a systematic difference between the absolute magnitudes of the 3CR and selected-region galaxies. We believe the first possibility can be discounted; our galaxies at $z \lesssim 1$ fit well on the 3CR K–z relation. Some evidence for a systematic shift in luminosity at high redshift may exist: Yates, Miller & Peacock (1986) have found a correlation between radio power and absolute magnitude in the most powerful 3CR radio galaxies. This would imply that the high-redshift galaxies in fainter samples such as the selected regions would have redshifts that are overestimated on the basis of the 3CR Hubble diagram. Indeed, with the exception of the galaxy at $z = 3.345$ (Lilly 1988), the very faint ($K \gtrsim 17.5$) galaxies in the 1-Jy sample with known redshifts do appear to be on average slightly underluminous. If real, this is only a small effect – and is in any case in the wrong direction to affect our conclusions. Only if our estimated redshifts were too *small* would it be possible to deduce a spurious redshift cutoff in the RLF. Although this possibility seems unlikely, we have constructed an *ad hoc* modification of the data set to illustrate the sort of errors which would be necessary for our conclusions to be

modified significantly. This is designed to mimic the form of curvature in the K–z relation which can arise through the choice of younger stellar evolution models (see Dunlop *et al.* 1989b for examples). A simple way of achieving such curvature is to modify the estimated redshifts z_e as follows: $(1+z_e)\rightarrow(1+z_e/\gamma)^\gamma$. For $\gamma=1.5$ this replaces redshift estimates of 2 and 3 by 2.5 and 4, respectively. This is certainly the sort of magnitude of error which one might worry about in practice. To avoid generating maximum redshifts too extreme for optical detection, we decided not to allow any of these modified estimates to exceed $z=5$. The resulting two candidate redshift distributions for the steep-spectrum sources in the selected regions are shown in Fig. 4 (the flat-spectrum redshift distributions are essentially unchanged). These two distributions will hereafter be referred to as the MEAN-z and HIGH-z distributions, respectively. The modelling described in this paper was performed using both redshift distributions in order to show how the results depend on the redshift estimation procedure.

Finally, it is clear that much of the remaining uncertainty in the high-redshift evolution of the RLF could be resolved by concentrating future spectroscopic efforts on those objects in the 2.7-GHz samples with potentially high redshifts. We have therefore considered very carefully every possible high-redshift candidate in the complete samples used here, and the resulting source lists (along with existing redshift estimates) are presented in Appendix B.

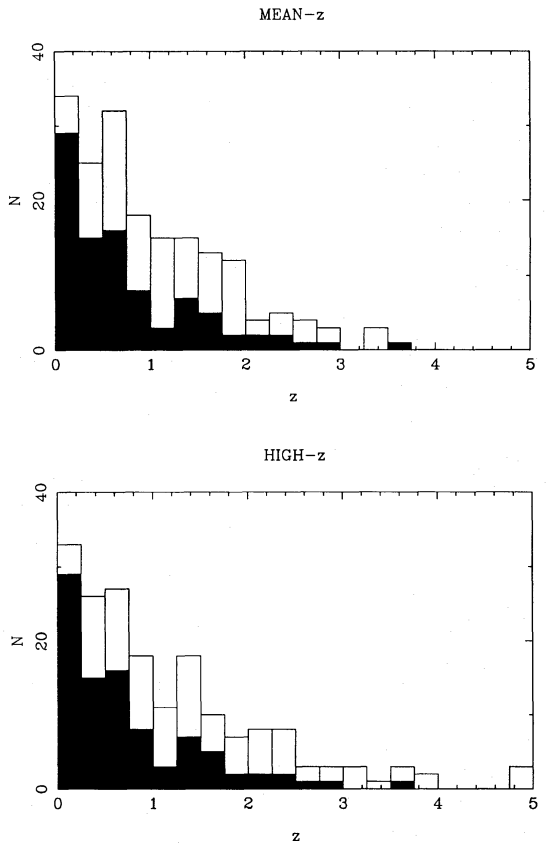

Figure 4. The MEAN-z and HIGH-z redshift distributions for the sources in the selected regions sample which result from redshift estimation procedures described in the text. The filled histogram shows spectroscopic redshifts, the open histogram the estimates.

3 MODELLING OF THE RLF, AND THE REDSHIFT CUT-OFF

3.1 Background

This section is mainly concerned with free-form modelling of the radio luminosity function (RLF) with the aim of determining what possible range of evolving luminosity functions is allowed by the data. The work described here represents an extension of the earlier work of Peacock (1985) in the light of the newly acquired data on the selected regions (Dunlop *et al.* 1989a). Of particular interest is the impact of the selected regions on the form of the high-redshift evolution.

Model fitting has proved to be a very valuable approach to the study of the radio luminosity function, chiefly because of the incomplete redshift information available in radio surveys. Since the redshift content of such surveys is generally only well defined at higher flux densities, the form of the RLF is well constrained only in the corresponding region of the P–z plane. A consistent model is of value, however, because it can extrapolate the trends which are observed in this region into less well-defined areas. Moreover, the form of this extrapolation is constrained by less complete data such as source counts and identification statistics. The model-fitting approach therefore allows maximum use to be made of all the available data.

The benefits of the free-form technique have been discussed by Peacock & Gull (1981) and Peacock (1985). Earlier attempts to model the RLF (e.g. Wall, Pearson & Longair 1980, 1981; Robertson 1978, 1980; Condon 1984) all involved preconceived assumptions as to the form of the evolution, and gave no indication as to how well the models were constrained by the data. In contrast, the aim of the free-form approach is to find an ensemble of different smooth functions which are consistent with the data. These models should agree in regions of the P–z plane where they are strongly constrained by high-quality data. However, the extrapolations of the various models into the ill-constrained regions will in general differ, and the hope is that the model ensemble will span approximately the uncertainty in smooth extrapolation of the existing data.

There is of course no guarantee that the model ensemble will describe the full range of possible extrapolations. However, where the models strongly diverge it is clear that the data are inadequate to constrain the form of the RLF. In the regions where the models agree, such agreement may be fortuitous but it is more likely that it may represent some genuine feature in the RLF. This possibility can then be checked by using the models to make falsifiable predictions which can be tested using a model-independent approach. This information can then be used to decide which data sets should be regarded as high priority for more detailed study. In fact, it was considerations of this sort that led to the choice of the selected regions as the most suitable sample capable of resolving the issue of the redshift cut-off for powerful radio sources.

3.2 Construction of the model RLFs

The technical aspects of model building are unchanged since Peacock (1985) and so a detailed description is not included here. The important features are as follows.

(i) The model RLFs are dual-population models. The steep-spectrum ($\alpha \geq 0.5$) and flat-spectrum ($\alpha < 0.5$) populations are treated as distinct and hence the corresponding RLFs are modelled independently.

(ii) The models are multi-frequency models. Although the derived model RLFs are defined at 2.7 GHz, data at other frequencies are used to help constrain them. To relate data at different frequencies it is necessary to incorporate the known correlation between spectral index and luminosity for steep-spectrum sources. The comparison of source counts in Section 2.2 shows that all steep-spectrum data are consistent with a mean spectral index of $\alpha \simeq 0.85$, which is slightly steeper on average than the model assumptions of Peacock (1985) (this problem is revealed by the improved accuracy of the 5-GHz data). Thus, the model spectra were steepened uniformly by 0.05. This makes a negligible change to the space densities obtained, but allows one to fit all the count data with one model RLF:

$$\begin{aligned} &P_{2.7} < 10^{24}\ \mathrm{W\ Hz^{-1}\ sr^{-1}}: \quad \alpha = 0.80 \\ &P_{2.7} > 10^{24}\ \mathrm{W\ Hz^{-1}\ sr^{-1}}: \quad \alpha = 0.80 \\ &\qquad\qquad + 0.015(\log_{10} P - 24)^2. \end{aligned} \tag{1}$$

For flat-spectrum sources $\langle\alpha\rangle = 0$ was assumed.

(iii) The overall goodness of fit of each model was assessed via the W statistic (Peacock 1985)

$$W = \prod_{i=1}^{n} p_i, \tag{2}$$

where p_i is the significance level of the ith data set (i.e. the probability that the misfit statistic for the ith data set would be larger than the observed value by chance). On the null hypothesis, the distribution of $-\ln W$ for large n will be normal with mean n and variance n (the exact distribution is

$$\frac{dp}{dx} = \frac{x^{(n-1)}}{(n-1)!}\, e^{-x}, \tag{3}$$

defining $x \equiv -\ln W$). This statistic is effective at detecting low values of P_i and hence ensures that no individual data set is very poorly reproduced by the model. The individual P_i's are calculated using the χ^2 statistic in the case of the binned data sets (i.e. source counts, identification data, local RLF – see Section 2.1) and using the two-dimensional Kolmogorov–Smirnov (KS) test (Peacock 1983) in the case of the complete-sample S–z distributions. Note, however, that the W statistic is not used to optimize the model, but merely to assess the final figure of merit. This is because the KS statistic does not vary sufficiently continuously in parameter space to be suitable for use in optimization, and so, in practice, the actual fitting of the S–z distributions is better achieved using the maximum likelihood technique (see Peacock 1985 for details of method of optimization).

(iv) All the models were constructed assuming a Friedmann cosmology with $\Omega_0 = 1$. However, it is not necessary to repeat the modelling for other cosmologies since the RLFs for two different geometries, ρ_1 and ρ_2 are related by

$$\rho_1(P_1, z)\frac{dV_1}{dz} = \rho_2(P_2, z)\frac{dV_2}{dz}, \tag{4}$$

where P_1 and P_2 are the luminosities derived from (S, z) using the corresponding effective distances in the two cosmologies, D_1 and D_2. The only complication is the variation of spectral index due to the $P-\alpha$ relation, since $P_1/P_2 = (D_1/D_2)^2$ which is a function of redshift [i.e. $\alpha = \alpha(P_1)$ implies $\alpha = \alpha(P_2, z)$ in the new geometry]. However, as argued by Peacock (1985), this redshift effect is unimportant unless P_1/P_2 becomes several orders of magnitude and in fact, for reasonable values of z and Ω_0, $0.5 \leq P_1/P_2 \leq 2$.

3.2.1 *The model RLF ensemble*

The RLF ensemble consists of five differently formulated models which were found to be consistent with the data. These are all 'free-form' models constructed in a similar manner to the RLFs of Peacock (1985). We have also attempted to fit the data using the less general assumptions of pure luminosity evolution and luminosity/density evolution; these models are discussed separately in Section 3.4.

Models 1–5 were all constructed using a series expansion

$$\log_{10}(\rho) = \sum_{i=0}^{n}\sum_{j=0}^{n-i} A_{ij} x^i(P)\, y^j(z), \tag{5}$$

where x and y are transformed axes of the P–z plane, and the series was truncated at the lowest expansion order consistent with the data. Model numbers 1 may be regarded as the fundamental model: the (P, z) coordinates are $[0.1(\log_{10}P - 20),\ 0.1\ z]$ and integration of the RLF is carried out over the redshift range $z = 0$–10, and over the luminosity range $P_{2.7} = 10^{18}$–10^{30} W Hz^{-1} sr^{-1}. The expansion orders are 5th order (21 terms) for the steep-spectrum RLF [plus one extra term in $(\log_{10}P)^6$ to assist in fitting the sharp kink in the local RLF] and 4th order (15 terms) for the flat-spectrum RLF. Models 2–5 vary successively one aspect of this, as shown below.

RLF2: an exponential cut-off is enforced at high luminosity: $\rho \rightarrow \rho \exp(-P/P_c)$, where $P_c = 10^{28}$ W Hz^{-1} sr^{-1} (as in Peacock 1985).
RLF3: the redshift coordinate used is $\log_{10}(1+z)$ instead of $0.1\ z$.
RLF4: integration of the RLF is terminated at $z = 5$ instead of $z = 10$.
RLF5: a cut-off at high redshift is enforced such that the RLF decays sinusoidally from $z = 2$ to a value of zero at $z > 5$, i.e. for $2 < z < 5$, $\rho \rightarrow \rho(1 + \cos\phi)/2$, where $\phi = (z-2)\pi/3$, and for $z \geq 5$, $\rho = 0$.

Models number 1–4 are directly comparable with models 1–4 of Peacock (1985). Peacock's model 5 involved enforcing zero evolution of the RLF out to $z = 0.4$. In view of the difficulty experienced in the present work in fitting the new local RLF at $z = 0.2$, this model was not re-attempted.

These models were each derived twice, using the two different versions of the database: the MEAN-z and HIGH-z estimates described in Section 2.5. This was done in order to test the sensitivity of the models to these estimated redshifts. It was found that all of the models could achieve acceptable fits (at better than the 1 per cent level) over all the data sets. The variations between the five model RLFs in each ensemble therefore give a lower bound to the 99 per cent confidence limits on $\rho(P, z)$.

The expansion parameters for models 1–5 derived on the basis of the MEAN-z and HIGH-z data sets are given in

Appendix C (Tables C1 and C2). All these models assume a density parameter $\Omega_0 = 1$, but as explained above, translation to other values is straightforward.

3.3 Model results

Results from the new model RLF ensemble are given in Fig. 5. These plots show the limits on ρ (allowed by the model RLFs) viewed at two different cuts of constant luminosity ($P_{2.7} = 10^{27}$ and 10^{26} W Hz^{-1} sr^{-1}) over the luminosity range in which the high-redshift RLF is reasonably well defined. The most important feature of these diagrams is that, independent of Ω_0, the new model RLFs show a turn-over at high-redshift in the steep-spectrum population which is not exhibited by the model RLFs of Peacock (1985). These new constraints on the high-redshift form of the steep-spectrum RLF are a direct consequence of the improvement in the steep-spectrum database provided by the addition of the Parkes selected regions sample. The new models also provide improved constraints on the form of the flat-spectrum cut-off.

The detailed behaviour of the RLF has several features worthy of comment. First, there is some suggestion that the redshift at which the RLF peaks is a function of luminosity; secondly, the steep-spectrum RLF appears to peak at a higher redshift than the flat-spectrum RLF. It is not clear how much importance should be attached to these features: if there was a luminosity dependence of peak redshift, then simple differences in spectral index ensures that $z_{\rm peak}(P)$ cannot be the same for flat-spectrum and steep-spectrum population at all frequencies. In fact, the luminosity evolution models investigated in Section 3.4 below indicate that such a dependence is not definitely required. As usual, the data only define the high-redshift RLF over a restricted range of power, so it is scarcely surprising that it is hard to settle this question.

The most important fact is that it now seems likely that the *whole* radio population (i.e. both flat- and steep-spectrum sources) suffers a gradual high-redshift decline over the redshift range $z \simeq 2$–4. The extent of the decline is quite modest: at $P_{2.7} = 10^{27}$ W Hz^{-1} sr^{-1}, where the constraints are probably best, the decline is only a factor of about $3(\Omega_0 = 1)/6(\Omega_0 = 0)$ for the flat-spectrum RLF and consistent with this for steep-spectrum sources.

Having found evidence for a high-redshift cut-off in the steep-spectrum RLF, it is important to consider the robustness of this result. Fig. 6 shows the results of the RLF models derived on the basis of the HIGH-z data sets, for comparison with the MEAN-z results which were presented in Fig. 5. As

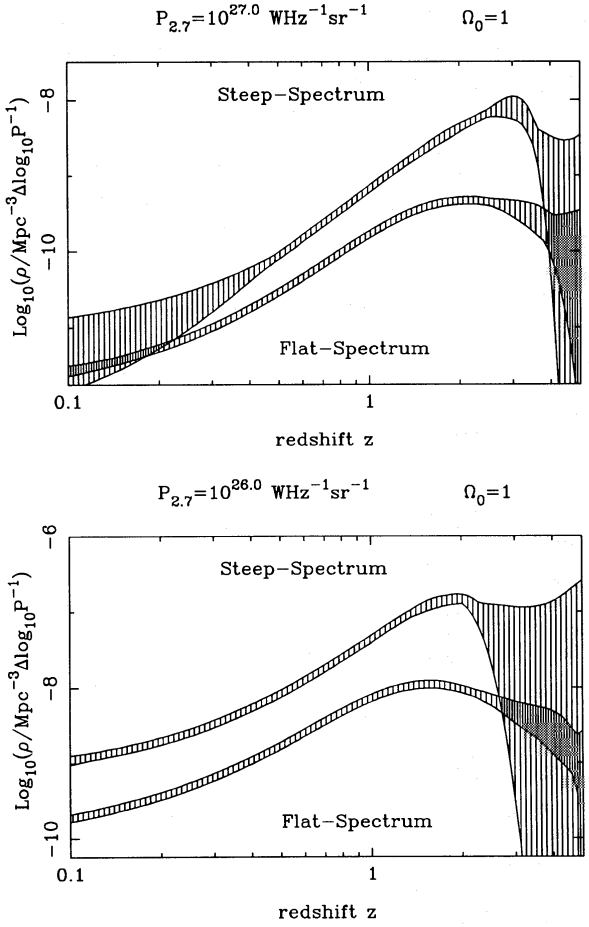

Figure 5. The limits to ρ at constant $P_{2.7}$ allowed by the new model RLFs (MEAN-z data set), for $\Omega_0 = 1$. $\mathrm{Log}_{10}(\rho)$ is plotted against redshift at two different luminosities $P_{2.7} = 10^{27}$ and 10^{26} W Hz^{-1} sr^{-1}. Units of ρ are Mpc^{-3} $(\Delta \log_{10} P_{2.7})^{-1}$. For low Ω_0 the appearance of the plots is almost identical, provided cuts are made at luminosities a factor of ~ 3 higher than those shown.

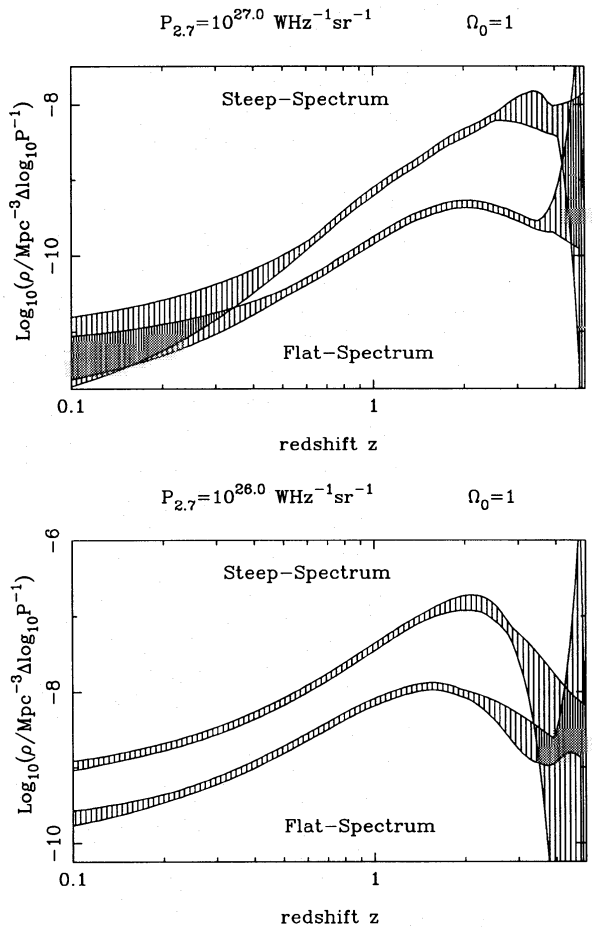

Figure 6. The limits to ρ at constant $P_{2.7}$ allowed by the new model RLFs derived using the HIGH-z redshift distribution for the selected regions. $\mathrm{Log}_{10}(\rho)$ ($\Omega_0 = 1$ only) is plotted against redshift at two different luminosities $P_{2.7} = 10^{27}$ and 10^{26} W Hz^{-1} sr^{-1}. Units of ρ are Mpc^{-3} $(\Delta \log_{10} P_{2.7})^{-1}$.

expected, the form of the flat-spectrum RLF is essentially unchanged because of the small fraction of sources in the complete samples which lack redshifts. However, the range of steep-spectrum RLFs allowed by the HIGH-z models is rather different, and, certainly at $P_{2.7} = 10^{27}$ W Hz^{-1} sr^{-1}, no longer displays an unambiguous turnover at $z \sim 2$, (although at $P_{2.7} = 10^{26}$ W Hz^{-1} sr^{-1} the cut-off actually appears firmer – see Section 4.3 for an explanation of this initially rather surprising result). It therefore seems feasible that a redshift cut-off in the steep-spectrum RLF would in fact not be required *if* the true redshift distribution of the selected regions were to be represented by the HIGH-z distribution. Although we have argued that there are good reasons for believing the HIGH-z redshift estimates to be unrealistic, it is disturbing nevertheless that such a relatively minor change in the data can perturb our conclusions so significantly.

3.4 Luminosity evolution models for the RLF

In the modelling described above no attempt was made to describe the evolution of the RLF by a simple parametric form, such as pure luminosity evolution, pure density evolution (PLE), or some combination of the two. Indeed, one of the objectives of the free-form modelling was to avoid as far as possible such preconceived assumptions concerning the form of evolution. However, given the recent interest in pure luminosity evolution as a model for the evolution of optically selected quasars (Koo 1986; Shanks *et al.* 1986; Marshall 1987; Boyle *et al.* 1987, 1988), it is interesting to explore whether this simple form is also an acceptable description of the evolving RLF.

For the two extreme possibilities of pure luminosity evolution and pure density evolution to be distinguished, the luminosity function must contain some feature whose progress with redshift can be monitored. Only then is it possible to determine whether the luminosity function shifts horizontally in the (P, ρ) plane with redshift (i.e. luminosity evolution) or vertically (i.e. density evolution). In the case of optically selected quasars such a feature is indeed present in the form of a 'break' in the optical luminosity function – at low luminosities the luminosity function is well described by a power law of relatively shallow slope ($P^{-0.25}$), but above some critical power ($P_c \equiv M_B = -21.8$) a steeper slope is required ($P^{-2.6}$). To investigate the movement of this feature with redshift it is necessary to study large samples of quasars which are faint enough to sample luminosities below the 'break', even at large redshifts. The recent results of Boyle *et al.* (1987, 1988) suggest that the luminosity function shifts horizontally in the (ρ, P) plane [parameterized by $P \propto (1+z)^k$, $k = 3.5 \pm 0.3$ for $\Omega_0 = 1$], consistent with the picture of pure luminosity evolution.

It is therefore of some interest to investigate whether pure luminosity evolution is consistent with the radio database which was used to construct the free-form models in Section 3.2. It is also interesting to consider the implications of pure luminosity evolution at high redshift. Because most of the optical studies are largely based on UVX quasars, the evolution of the quasar optical luminosity function has only been investigated out to $z \sim 2$. As stated above, this evolution can be parameterized by $(1+z)^k$ and so is consistent with continuing *positive* luminosity evolution out to $z \sim 2$. However, since we have established that the RLF appears to decline at high redshift, a pure luminosity evolution model of the RLF cannot continue to evolve in the same direction beyond $z \sim 2$. Either the direction of luminosity evolution must reverse, or a depression in comoving density must occur at high redshift. These possibilities are investigated below.

3.4.1 *A model of pure luminosity evolution*

The model of luminosity evolution was formulated as follows. The RLF was considered to be the sum of two components, a high-power evolving component ρ_h, and a low-power non-evolving component ρ_l. Physically, the idea here is to try to fit PLE to the powerful elliptical radio galaxy population (described by ρ_h), while assuming no evolution for the spiral/irregular galaxy population (described by ρ_l) which dominates at the lowest radio powers. At least for the steep-spectrum population, such an assumption is certainly needed: luminosity evolution of the whole RLF cannot fit the data. So, our model consists of

$$\rho_t(P, z) = \rho_l(P) + \rho_h(P, z). \tag{6}$$

ρ_h is the evolving two-power-law RLF, analogous to the evolving quasar optical luminosity function:

$$\rho_h = \rho_0 \left\{ \left(\frac{P}{P_c(z)} \right)^{\alpha} + \left[\frac{P}{P_c(z)} \right]^{\beta} \right\}^{-1}, \tag{7}$$

where α and β are the two power-law slopes, $P_c(z)$ is the evolving 'break' luminosity, and ρ_0 is determined by normalization at $z = 0$.The redshift dependence of P_c was parameterized as a quadratic in order to permit the possibility of negative luminosity evolution at high redshift, i.e.

$$\log_{10}[P_c(z)] = a_0 + a_1 z + a_2 z^2. \tag{8}$$

ρ_l was parameterized as a power-law expansion in luminosity (terminated after the same number of terms as in the case of the free-form modelling), i.e.

$$\log_{10}(\rho_l) = \sum_{i=0}^{6} b_i x_P^i, \tag{9}$$

where $x_P \equiv 0.1(\log_{10} P - 20)$.

As in the free-form modelling, the flat- and steep-spectrum RLFs were modelled independently and a density parameter of $\Omega_0 = 1$ was assumed. An acceptable fit was achieved at the same level (i.e. ~ 1 per cent) as that achieved by the free-form models (see Section 3.3); the best-fitting model parameters are given in Table C3. Moreover, in the case of the flat-spectrum RLF, ρ_l was found to be superfluous since the fitted low-power section of ρ_h (i.e. $P^{-0.88}$) is itself consistent with the flat-spectrum local RLF. Comparison with the local RLF data shown in Fig. 1 shows that no extra-low power component is required in the flat-spectrum RLF, but in the steep-spectrum case, ρ_l is necessary to model the structure seen at lower powers. This empirical result may be understood as reflecting the known fact that, whereas the flat-spectrum local RLF continues to be dominated by elliptical galaxies down to low powers, the steep-spectrum local RLF contains additional spiral and irregular galaxy components at low power. ρ_h could there-

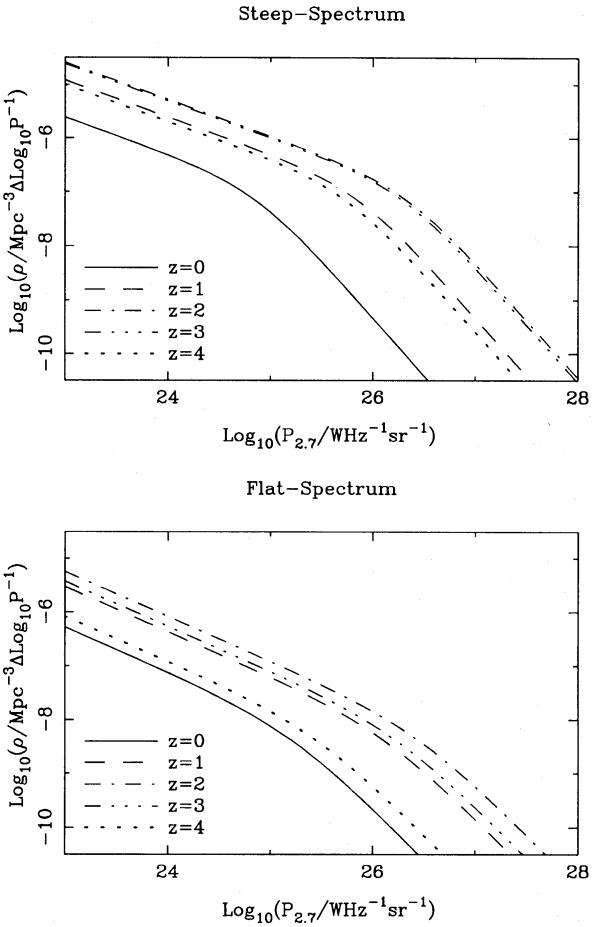

Figure 7. The evolving RLF predicted by the pure luminosity evolution model (MEAN-z data). $\mathrm{Log}_{10}(\rho)$ is plotted against $\log_{10}(P)$ at $z = 0, 1, 2, 3, 4$.

fore be interpreted as the luminosity function of elliptical radio galaxies.

The results of the luminosity evolution model for MEAN-z data are presented in Fig. 7, in which the model RLF is shown at various redshifts. Both flat- and steep-spectrum RLFs display positive luminosity evolution out to $z \sim 2$, but by $z \sim 3$ the evolution has reversed, and at $z \sim 4$ the RLF is approaching the local value once again (the flat-spectrum behaviour is remarkably symmetric in redshift space). These results are therefore consistent with a decline in comoving density at a given luminosity beyond $z \sim 2$. It is interesting that this simple model, with its much smaller number of free parameters, provides almost as good a fit to the data as was achieved by the truly free-form models of Section 3.2.

Following this successful fitting of pure luminosity evolution with $\Omega_0 = 1$, we tried the same model assuming $\Omega_0 = 0$. A successful fit (i.e. $P > 0.01$) was not achieved in the new geometry (in fact $P < 10^{-5}$). This result is sensible because it is clear that pure luminosity evolution should not be able to work for all values of Ω_0. Note that in contrast to this, Boyle *et al.* (1987, 1988) claimed to be able to fit pure luminosity evolution to the quasar optical luminosity function in both critical and empty universes. This fact may seem to indicate that the form of the evolving RLF is better constrained at present than the form of its optical quasar counterpart, but it is probably also due to the extra sensitivity to cosmology which results from probing out to redshifts $z > 2$.

Finally, as with the free-form models, we attempted to fit this model to the HIGH-z data set. An acceptable fit was not achieved, for reasons we discuss below.

3.4.2 *Alternative forms of evolution at high redshift*

Because of the restriction of pure luminosity evolution, the model described in the previous section is obliged to display negative luminosity evolution beyond $z \sim 2$ in order to conform with the high-z cut-off. However, continuing positive luminosity evolution beyond $z \sim 2$ could possibly be reconciled with the redshift cut-off, if it were combined with negative density evolution. The motivation for considering this form of high-redshift evolution is that it naturally results in a redshift cut-off which is differential in radio power, and hence predicts that any radio sources discovered at very high redshifts (i.e. $z \sim 3$–4) are likely to be extremely luminous. Such an effect would explain why PKS 1351 − 018, which is the most distant known object in the selected regions, has a radio flux density a factor of 10 higher than the limit of the survey.

To investigate the possibility of such luminosity/density evolution (LDE) at high z, the pure luminosity evolution model of Section 3.4.1 was modified to allow ρ_0 to vary with z. The adopted form was simply a polynomial in y_z:

$$\log_{10}[\rho_0(z)] = \sum_{i=0}^{5} c_i y_z^i. \qquad (10)$$

Since we were especially interested in whether there was any evidence for the break luminosity continuing to brighten at high redshift, the luminosity evolution of the break was constrained to be positive only. The dependence obtained when using $\log_{10} P_c = a_0 + a_1 z$ appears to be too extreme, although milder evolution of the form $\log_{10} P_c = a_0 + a_1[1 - (1+z)^{-\eta}]/\eta$ could be successfully accommodated.

Once again $\Omega_0 = 1$ was assumed and we tried to fit the model to both MEAN-z and HIGH-z data sets; we were successful in both cases, although the fit to the MEAN-z data was superior. The best-fit parameters are given in Table C4 and the results (for the MEAN-z data) are presented in Fig. 8.

We can understand why the PLE model failed to fit the HIGH-z data, whereas the LDE model was able to account for both MEAN-z and HIGH-z data, as follows. Examination of Figs 5 and 6 shows that there is a tendency for the free-form models to peak at higher redshifts for higher powers. This trend is weak in the MEAN-z data, but strongly enhanced in the HIGH-z data. The LDE model, being more general, is able to follow this behaviour. If the MEAN-z data are correct, then to distinguish between PLE and LDE requires new data, to explore evolution of the RLF around and below the break luminosity. We discuss some future possibilities in Section 4.4.

4 DIRECT INVESTIGATION OF HIGH-REDSHIFT EVOLUTION

4.1 Coverage of the P–z plane and direct plots of the RLF

The evidence for the high-redshift cut-off presented in the previous section was based on model fitting. However, as was

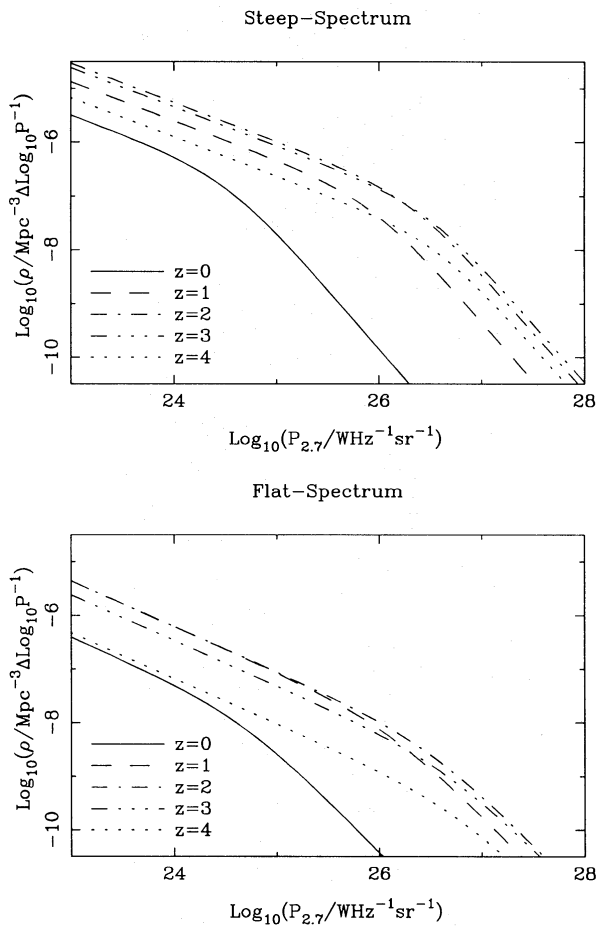

Figure 8. The evolving RLF predicted by the luminosity/density evolution model (MEAN-z data). $\mathrm{Log}_{10}(\rho)$ is plotted against $\log_{10}(P)$ at $z = 0, 1, 2, 3, 4$.

stressed in the introduction to that section, it is important to try to investigate in a model-independent manner the features which are displayed by the model RLFs. We cannot be sure of the reality of the redshift cut-off unless its existence can be deduced directly from the data. Fig. 9 illustrates the coverage of the P–z plane provided by the complete sample data at 2.7 GHz. Sources with estimated redshifts (and hence estimated luminosities) are shown on these plots as open circles, and the flux-density limits of the various individual samples appear as diagonal lines.

These diagrams emphasize the crucial role of the selected regions sample in making accessible a region of high-redshift space which could be occupied by typical high-luminosity radio sources. It is clear that the previous steep-spectrum flux limit of 1.5 Jy prohibits detection of even the most powerful radio sources ($P_{2.7} \simeq 10^{28}$ W Hz^{-1} sr^{-1}) beyond $z \simeq 2.5$, whereas the addition of the selected regions sample allows us to detect sources with $P_{2.7} > 10^{27}$ W Hz^{-1} sr^{-1} at redshifts > 3, should they exist. It is the relative lack of such high-luminosity high-redshift sources in Fig. 9 which produces the redshift cut-off displayed by the models in the previous section. Fig. 9 also shows the range of luminosities for which the selected regions sample allows us to reach any conclusion regarding high-redshift evolution – fainter samples are necessary before any statement can be made concerning the behaviour of sources with $P_{2.7} \lesssim 10^{25.5}$ W Hz^{-1} sr^{-1} at $z \gtrsim 2$.

If the coverage of the P–z plane shown in Fig. 9 was more complete, it would be relatively simple to investigate the evolving RLF by simple binning of the data in luminosity and redshift. This direct approach has been used in studies of the optical luminosity function of quasars (e.g. Boyle *et al.* 1987, 1988) where good coverage of the P–z plane is relatively easily achieved for $z < 2$. In comparison, the coverage of the P–z plane in the radio remains relatively sparse, despite the improvement which has resulted from the addition of the selected regions sample. Simple binning makes inefficient use of these data; hence the extensive modelling described in Section 3. Nevertheless it is instructive to attempt a direct determination of the evolving RLF from the complete sample data, and the results of this calculation are shown in Fig. 10. This figure should be regarded as no more than illustrative, since redshift resolution has been sacrificed in achieving significant numbers of objects per bin, but it compares very well with, for example, the predictions of the pure luminosity model shown in Fig. 7, and shows (in a relatively transparent manner) the slope and evolution of the RLF. Even in the raw P–z data there is clear evidence for a break in the luminosity function, together with evolution which approximates to pure luminosity evolution (at least out to $z \simeq 2$).

4.2 A simplified model

Before proceeding with a general analysis, it is illuminating to consider a simple model which allows some insight into the sensitivity of our conclusions on the redshift cut-off to the presence or absence of a few distant objects.

While the volume elements at high redshift do not fall particularly rapidly, the dimming of objects at high redshift becomes rapid for objects with steep spectra, which is one reason why it has proved easier to constrain the flat-spectrum population. Also, if the RLF is very steep at the high-luminosity end then, in a flux-limited sample, high-redshift objects are rapidly pushed to high powers and therefore low comoving densities. We can analyse this as follows. Let the RLF be a power law

$$\rho \propto P^{-\beta}, \tag{11}$$

in which case the integral comoving density of objects more luminous than P is also proportional to $P^{-\beta}$. In a flux-density limited sample, there is a redshift-dependent luminosity limit

$$P_{\mathrm{lim}} = S_{\mathrm{lim}} D^2 (1+z)^{1+\alpha}, \tag{12}$$

where $D/(1+z)$ is angular-diameter distance. Hence, with a comoving volume element

$$dV \propto D^2 \frac{dz}{(1+z)\sqrt{1+\Omega z}}, \tag{13}$$

the differential redshift distribution expected is

$$\frac{dN(z)}{dz} \propto D^{2-2\beta}(1+z)^{-\beta(1+\alpha)-1}(1+\Omega z)^{-1/2}. \tag{14}$$

The abundance of high-redshift objects is mainly governed by the central term on the right-hand side of (14), which shows clearly the problems which arise with steep spectra and steep luminosity functions.

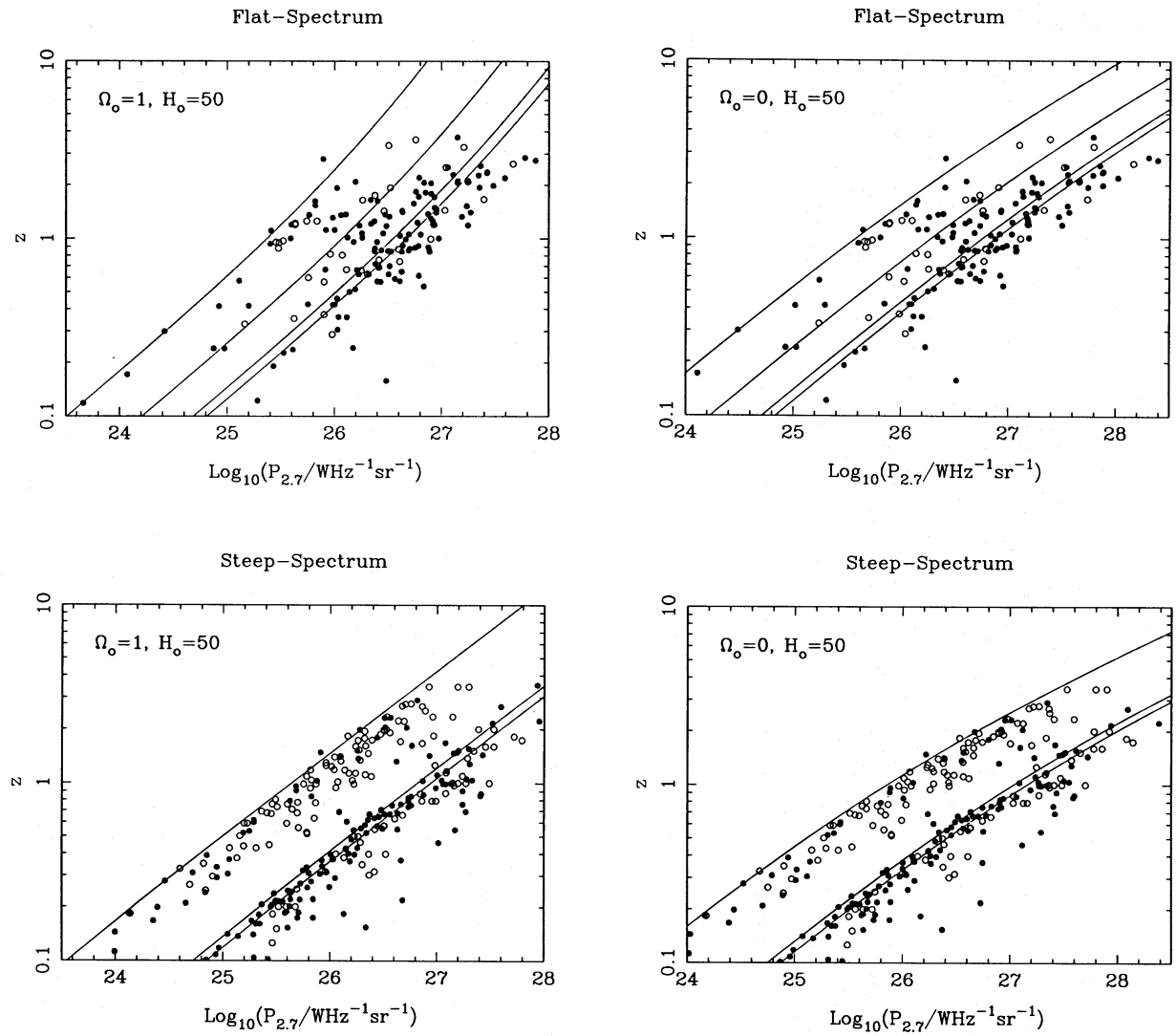

Figure 9. The coverage of the P–z plane provided by the complete sample database at 2.7 GHz (see Section 2.4). The open circles are sources with estimated redshifts (MEAN-z estimates for galaxies discussed in Section 2.5) and the diagonal curves are the flux density limits of the individual samples. The four separate plots show the flat- and steep-spectrum samples for both $\Omega_0 = 1$ and $\Omega_0 = 0$.

To compare with observations, we have fitted the form

$$\frac{dN}{dz} \propto (1+z)^{-\varepsilon} \qquad (15)$$

to the high-redshift data. For $z \geq 2$, we obtain maximum-likelihood values for ε of 7.5 ± 1.3 (flat-spectrum) and 6.6 ± 1.2 (steep-spectrum). The abundance of high-redshift objects clearly declines very rapidly. There is some weak evidence for curvature at the high-redshift end: for $z \geq 2.3$, we obtain $\varepsilon = 7.6 \pm 1.8$ (flat-spectrum) and 8.7 ± 1.9 (steep-spectrum). Is there any evidence for a cut-off from these figures? If we take $\beta = 2$ from Wall & Peacock (1985) (*cf.* Fig. 10), adopt the mean values of α for sources with $z \geq 2$ (0.87 and 0.13 for steep- and flat-spectrum, respectively), and say that, over the range $z = 2$–4, $D \propto (1+z)^{1-\Omega/2}$ is a reasonable approximation, then we predict $\varepsilon = 5.3 - \Omega/2$ (flat-spectrum) and $\varepsilon = 6.7 - \Omega/2$ (steep-spectrum). The observed redshift distributions do decline more rapidly than this, but the evidence for a cut-off for the steep-spectrum population is not very significant. Use of the HIGH-z data (at $z \geq 2$) yields $\varepsilon = 6.1 \pm 1.0$ (flat-spectrum) and $\varepsilon = 5.4 \pm 0.7$ (steep-spectrum), which totally removes even a hint of a steep-spectrum cut-off. We can now understand why the effect of the HIGH-z data on the free-form models was so dramatic: the expected numbers of high-redshift objects decline sufficiently rapidly that even a few objects assigned spurious high redshifts can greatly alter our inferred space densities.

Since any evidence for a cut-off from the redshift distribution depends critically on the value of β, it may be better to determine this self-consistently rather than relying on an external study. Accordingly, we have used the parametric form $\rho \propto P^{-\beta}(1+z)^{-\gamma}$ and deduced confidence limits on β and γ using maximum likelihood. These contours are shown in Fig. 11, and reinforce the above conclusions: the preferred value of β is $\lesssim 2$ and γ is positive. Note, however, that γ appears to be larger for the flat-spectrum population than it is for steep-spectrum sources.

It is worth contrasting this situation with optical searches for high-redshift quasars. Here the luminosity function can be much less steep if one surveys faint enough. Even so, the work of Warren *et al.* (1988) over 30 deg^2 at the SGP found

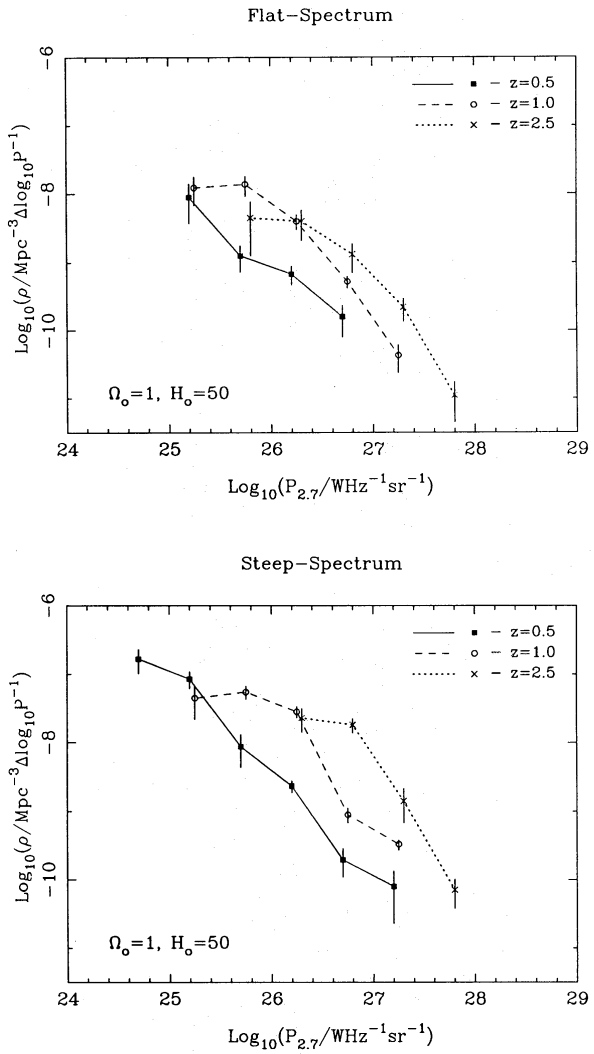

Figure 10. The evolving RLF produced by direct redshift and luminosity binning of the data shown in Fig. 9. $\mathrm{Log_{10}}(\rho)$ is plotted against $\log_{10}(P)$ at $z=0.5$, 1.0 and 2.5 for both flat- and steep-spectrum sources (for $\Omega_0=1$ only). These plots can only be regarded as illustrative because resolution in redshift space has been severely compromised to produce a reasonable number of objects per bin (the width of each redshift bin is 0.2 in $\log_{10}z$). Nevertheless these plots compare very well with the pure luminosity-evolution model predictions shown in Fig. 7, and illustrate clearly the extent to which the raw data can constrain the form of the RLF at large z.

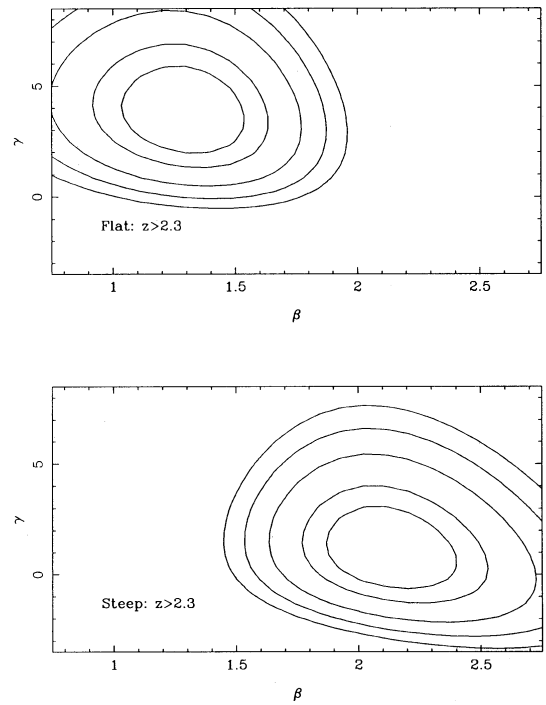

Figure 11. Contours of relative likelihood $\ln(L/L_{\max})$ for the model $\rho \propto P^{-\beta}(1+z)^{-\gamma}$ fitted to the complete-sample data at $z>2.3$. To ensure that a power-law approximation for the RLF is reasonable, only the region $10^{26}<P_{2.7}<10^{28}$ W Hz^{-1} sr^{-1} was considered. This diagram assumes $\Omega_0=1$; for $\Omega_0=0$, the values of γ would be lower by about 0.5. Contours are plotted at $-\ln(L/L_{\max})=0.5$, 1, 2, 3, 4. These correspond to two-dimensional confidence limits of 39, 63, 86, 95 and 98 per cent on a Gaussian approximation, or 68, 84, 95, 98.5, 99.5 per cent if one of the parameters is determined externally.

only three objects with $z>4$ at $R<20$ – out of a total of roughly 1000 quasars to that magnitude limit. Again, this is for a luminosity function that they believe to be declining only slowly – illustrating just how few high-redshift objects are required to define a significant density.

4.3 Quantifying the cut-off via the $V/V_{\max}$ test

Although the model results of the previous section give a useful feel for the behaviour of the RLF, it is clearly vital to be able to perform a model-independent investigation of high-redshift evolution. The most familiar way of achieving this is to use the $V/V_{\max}$ test (developed independently by Schmidt 1968, and Rowan-Robinson 1968). V is the cosmological volume enclosed by an object and $V_{\max}$ is the volume that would be enclosed by the same object if it were pushed out to the flux-density limit of its parent sample. Under the null hypothesis of uniform distribution in space, the individual values of $V/V_{\max}$ for objects in a flux-limited sample should be uniformly distributed between 0 and 1, and $\langle V/V_{\max}\rangle$ should be $0.5\pm(12N)^{-0.5}$, where N is the number of objects in the sample. Values of $\langle V/V_{\max}\rangle>0.5$ indicate a bias of objects towards the more distant regions of their accessible volumes, and hence correspond to an increase in comoving density with redshift. Conversely, values <0.5 indicate a deficit of high-redshift objects. This test has been applied to many radio samples over the years in order to demonstrate the strong positive evolution of radio sources between $z=0$ and $z\sim2$. Generally, values in the range 0.6–0.7 have been found (e.g. Wills & Lynds 1978; Peacock *et al.* 1981) – as demonstrated by Longair (1978), $\langle V/V_{\max}\rangle=0.7$ implies a density increase over present-day numbers at $1<z<3$ of ~1000.

The $V/V_{\max}$ test can therefore also be used to quantify the existence or otherwise of negative evolution beyond $z\sim2$. For the present study the basic test had to be modified in two ways. First, in order to apply the test to the complete combined 2.7-GHz samples the coherent V_e/V_a statistic of Avni & Bahcall (1980) was used. This is a generalization of the classical test which enables analysis of a combined sample in which V_e (volume enclosed) and V_a (volume available) are volumes which depend on the survey depth as a function of sky area. Secondly, in order to avoid any high-redshift negative evolution being masked by the known

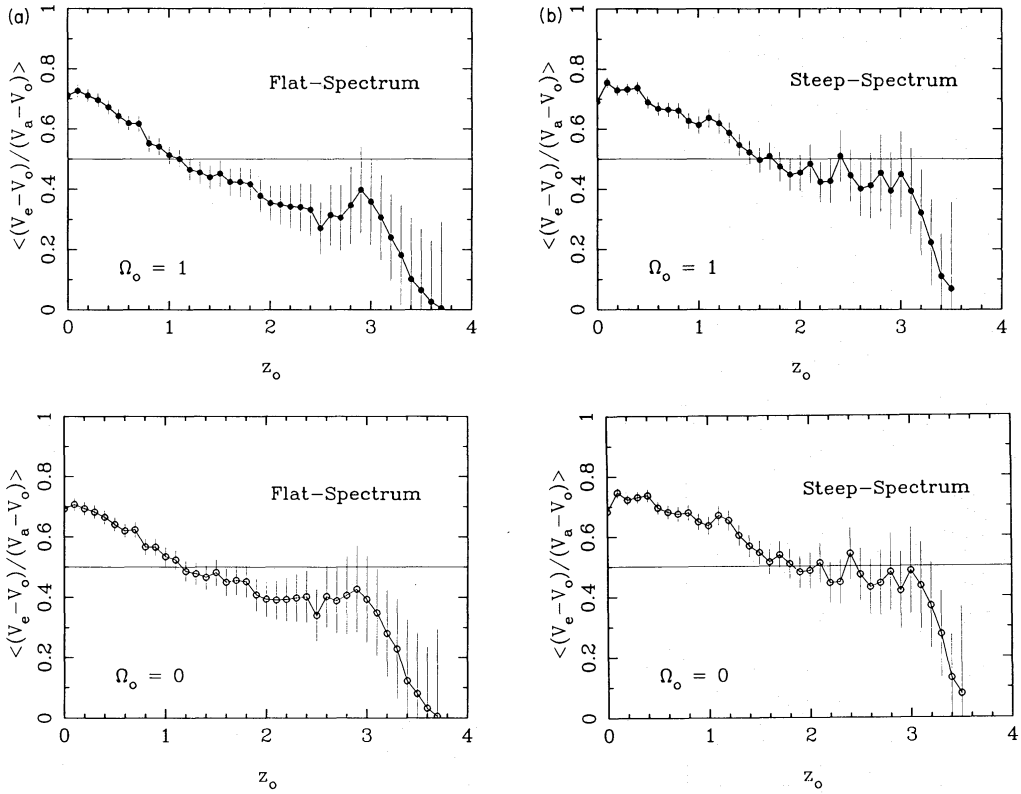

Figure 12. Plots of the banded V/V_{max} statistic $\langle (V_e - V_0)/(V_a - V_0)\rangle$ against z_0. The horizontal line in each plot indicates the value of 0.5 expected under the null hypothesis of zero evolution, and the statistical error bar associated with each point is given by $(12N)^{-0.5}$, where N is the number of objects left in the subsample with $z > z_0$. The plots were derived assuming the reduced area of 0.05 sr for the faintest bin in the selected regions sample (see Section 2.2). These results are presented in numerical form in Table 3, where they are also further subdivided into galaxy and quasar subclasses. (a) Complete flat-spectrum sample, assuming MEAN-z estimated redshifts. (b) Complete steep-spectrum sample, assuming MEAN-z estimated redshifts.

strong, positive, low-redshift evolution described above, a banded version of the test was required (Osmer & Smith 1980; Avni & Schiller 1983), i.e.

$$\langle V_e/V_a\rangle \rightarrow \left\langle \frac{V_e - V_0}{V_a - V_0} \right\rangle , \qquad (16)$$

where V_0 is the cosmological volume enclosed by a redshift z_0. We present the results of this banded V_e/V_a calculation in a series of plots of $\langle (V_e - V_0)/(V_a - V_0)\rangle$ against z_0 – Figs 12(a)–13(d). In producing all of these plots we have adopted the reduced area of 0.05 sr for the faintest bin of the selected regions sample (see Section 2.2); restoring the area to 0.075 sr simply reduces the values of V_e/V_a by $\simeq 0.03$.

The basic results for the complete flat- and steep-spectrum MEAN-z samples are shown in Figs 12(a) and (b), and are provided in numerical form in Table 3. These figures show clearly the high positive evolution of both flat- and steep-spectrum populations at 'low' redshift (i.e. while $z_0 < 1$), and, more importantly, also provide model-independent evidence of a high-redshift cut-off for *both* populations; for $z_0 > 2$ the values of $\langle (V_e - V_0)/(V_a - V_0)\rangle$ are almost always < 0.5 for both flat- and steep-spectrum sources irrespective of geometry (although for $\Omega_0 = 1$ the result is always stronger). Also provided in Table 3 is the further breakdown of these numbers into galaxy and quasar subclasses, showing that the cut-off applies to each of these individual subclasses (and thus cannot be due to, e.g., reclassification of flat-spectrum quasars as steep-spectrum at high z, as suggested by Savage & Peterson 1983).

However, the $(12N)^{-0.5}$ error bars shown in these diagrams make it clear that, as suggested by the modelling, the flat-spectrum cut-off is more secure than its steep-spectrum counterpart. It is therefore interesting to investigate the robustness of the steep-spectrum results, and this is done in the Fig. 13 (for brevity we only show results for $\Omega_0 = 1$; for $\Omega_0 = 0$ the values are typically $\simeq 0.03$ higher at high z). In Fig. 13(a) we show the effect of restricting our attention to a particular luminosity range of steep-spectrum sources; $P_{2.7} = 10^{26}$–10^{27} W Hz^{-1} sr^{-1} for $\Omega_0 = 1$, and $P_{2.7} = 10^{26.5}$–$10^{27.5}$ W Hz^{-1} sr^{-1} for $\Omega_0 = 0$. Comparison of Figs 12(b) and 13(a) shows that this luminosity binning has improved the significance of the steep-spectrum cut-off, indicating that the apparent weakness of the cut-off in Fig. 12(b) is due to a small number of very high-luminosity sources at large estimated redshifts. This may well be telling us that even some of the MEAN-z estimates are artificially high (since an excessive redshift estimate will yield an artificially high luminosity for a typical source whose flux density is not very close to the 0.1 Jy sample flux limit). Of course, if spectroscopy should confirm these large redshift estimates, such luminosity-dependent $\langle (V_e - V_0)/(V_a - V_0)\rangle$ results would then be suggestive of a luminosity-dependent cut-off.

The next variation to consider is the obvious one of repeating the $\langle (V_e - V_0)/(V_a - V_0)\rangle$ analysis for the HIGH-z

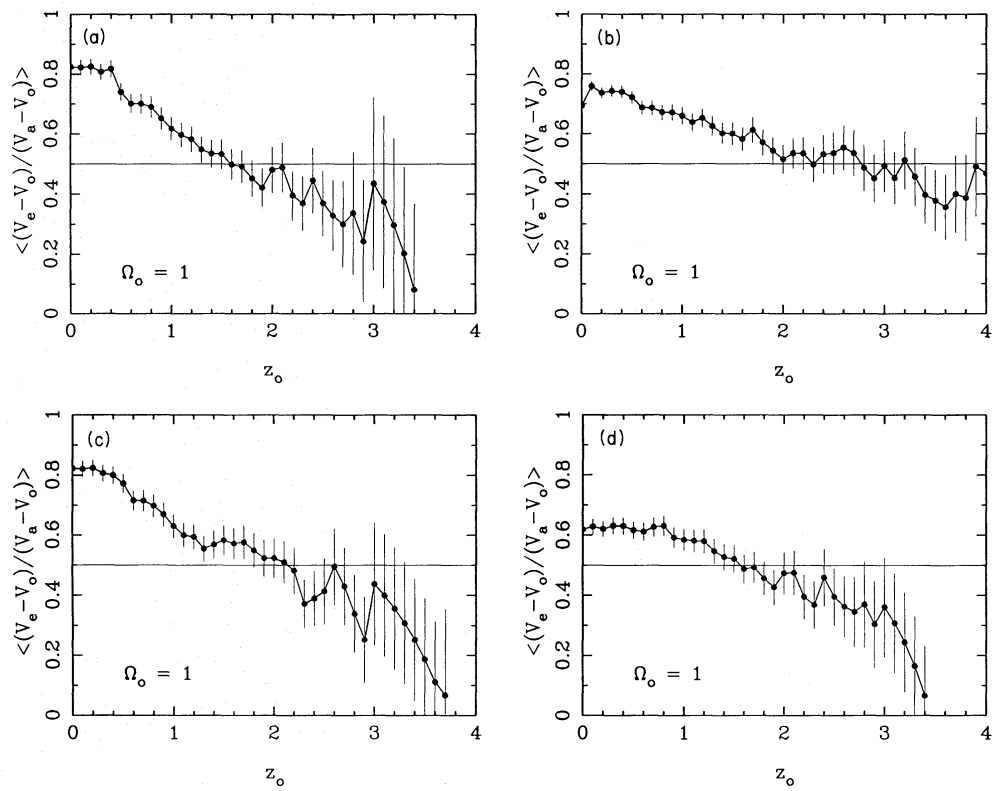

Figure 13. Exploring the robustness of the steep-spectrum $\langle (V_e - V_0)/(V_a - V_0) \rangle$ results. As in the previous figure the horizontal line in each plot indicates the value of 0.5 expected under the null hypothesis of zero evolution, and the statistical error bar associated with each point is given by $(12N)^{-0.5}$, where N is the number of objects left in the subsample with $z > z_0$. All plots were derived assuming the reduced area of 0.05 sr for the faintest bin in the selected regions sample (see Section 2.2). For brevity we show results for $\Omega_0 = 1$ only; as can be seen from the previous figure the results for $\Omega_0 = 0$ are typically $\simeq 0.03$ higher. (a) Complete steep-spectrum sample, assuming MEAN-z estimated redshifts as for Fig. 12, but this time limited to a restricted range of luminosity $P_{2.7} = 10^{26}$–10^{27} W Hz^{-1} sr^{-1}. (b) Complete steep-spectrum sample, assuming HIGH-z estimated redshifts. (c) Complete steep-spectrum sample, again assuming HIGH-z estimated redshifts, but this time considering only the same restricted luminosity range as in Fig. 13(a). (d) Selected regions steep-spectrum sample only, assuming MEAN-z estimated redshifts.

steep-spectrum sample. Fig. 13(b) shows the results of this calculation without any luminosity binning, and Fig. 13(c) shows the results with the luminosity range restricted as in Fig. 13(a). Comparison of Figs 13(b) and 12(b) make it clear that the adoption of the HIGH-z estimates has effectively removed the cut-off, again emphasizing how sensitive the results are to the existence of only a few objects at very high redshift. Interestingly, however, comparison of Figs 13(c) and 13(a) reveals that, when a restricted luminosity range is considered, the HIGH-z estimates *do not* remove all evidence for the cut-off. As above, this indicates that the V_e/V_a cut-off 'result' is being weakened by the (perhaps artificially) high-redshift estimates for a few relatively bright sources. This idea gains further support from our final V_e/V_a calculation shown in Fig. 13(d), which is the equivalent plot to Fig. 12(b) but this time restricted to just the selected regions sample (i.e. steep-spectrum, MEAN-z, no luminosity binning). Comparison with Fig. 12(b) shows that the selected regions alone provide cleaner evidence of a cut-off than does the combined 2.7-GHz database.

These model-independent calculations illustrated in Figs 12(a)–13(d) reinforce the conclusions obtained from the free-form modelling and the simple model of the previous subsection. In fact, we can make a quantitative comparison, by evaluating $\langle (V_e - V_0)/(V_a - V_0) \rangle$ for our $\rho \propto P^{-\beta}(1+z)^{-\gamma}$ model. The results may be approximated to better than 0.01 over the parameter regime of interest by the following empirical fitting formula:

$$\langle (V_e - V_0)/(V_a - V_0) \rangle \simeq \tfrac{1}{2}(1 + \gamma/\beta^b)^{1/2},$$
$$a = 0.31 + 0.05\,\Omega_0 - 0.14\,\alpha, \qquad (17)$$
$$b = 1.57 - 0.17 z_0.$$

A given value of γ thus produces a V/V_{max} closer to 0.5 for steep spectra; again it is easier to establish a cut-off for flat-spectrum sources. For example, $(\alpha, \beta, \gamma, \Omega, z_0) = (0.9, 2, 4, 1, 2)$ implies $\langle (V_e - V_0)/(V_a - V_0) \rangle = 0.42$. The simple model and V/V_{max} test are telling us much the same thing about the high-redshift behaviour of the RLF.

4.4 Predicted numbers of high-redshift objects

To finish, it is interesting to anticipate the impact of other samples on the models presented here, with the aim of seeing whether some of the uncertainties discussed above may be resolved.

4.4.1 The 1-Jy sample

At the high-redshift end, it is interesting to consider the 1-Jy sample (Allington-Smith 1984); this contains the second highest redshift radio galaxy so far published (0902 + 34 at

Table 3. $\langle V_e/V_a \rangle$ results (MEAN-z estimated galaxy redshifts).

i) All Sources

		Flat−spectrum $\langle V_e/V_a \rangle$			Steep−spectrum $\langle V_e/V_a \rangle$	
Redshift range	n	$\Omega_0=1$	$\Omega_0=0$	n	$\Omega_0=1$	$\Omega_0=0$
> 1.8	31	0.406	0.442	33	0.474	0.508
> 1.9	28	0.378	0.408	29	0.447	0.480
> 2.0	24	0.354	0.394	23	0.454	0.485
> 2.1	19	0.348	0.391	19	0.484	0.511
> 2.3	13	0.340	0.398	15	0.426	0.447
> 2.5	11	0.271	0.340	11	0.401	0.472

ii) Quasars only

		Flat−spectrum $\langle V_e/V_a \rangle$			Steep−spectrum $\langle V_e/V_a \rangle$	
Redshift range	n	$\Omega_0=1$	$\Omega_0=0$	n	$\Omega_0=1$	$\Omega_0=0$
> 1.8	28	0.417	0.452	10	0.519	0.537
> 1.9	26	0.382	0.413	10	0.463	0.482
> 2.0	22	0.364	0.407	9	0.432	0.450
> 2.1	18	0.355	0.398	7	0.470	0.492
> 2.3	12	0.355	0.416	5	0.432	0.447
> 2.5	10	0.291	0.366			

iii) Galaxies only

		Flat−spectrum $\langle V_e/V_a \rangle$			Steep−spectrum $\langle V_e/V_a \rangle$	
Redshift range	n	$\Omega_0=1$	$\Omega_0=0$	n	$\Omega_0=1$	$\Omega_0=0$
> 1.8	3	0.308	0.339	23	0.454	0.495
> 1.9	2	0.327	0.346	19	0.439	0.479
> 2.0	2	0.237	0.251	14	0.468	0.507
> 2.1				12	0.492	0.522
> 2.3				10	0.423	0.447
> 2.5				8	0.376	0.404

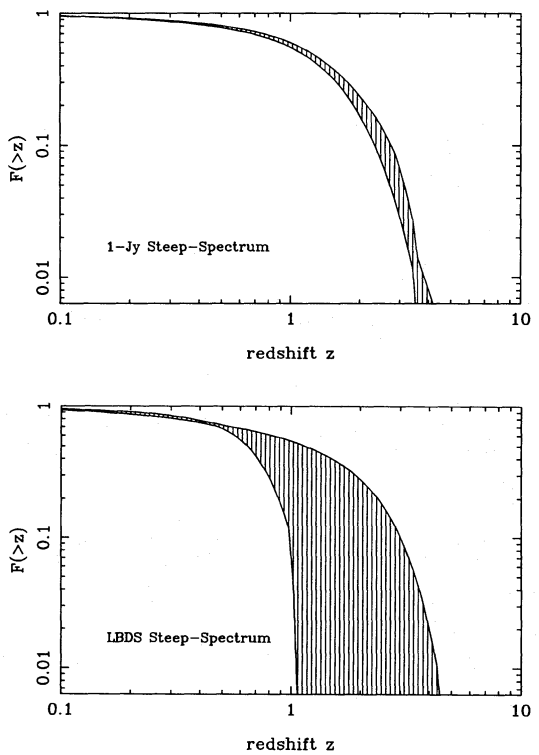

Figure 14. Predicted redshift distributions using the full ensemble of RLFs. (a) The 408-MHz 1-Jy sample. Note the close agreement of all models for $z \lesssim 3.5$. (b) The LBDS sample. Note the total lack of predictive power for $z \gtrsim 0.7$.

$z = 3.395$; Lilly 1988). The detailed redshift predictions of our models for this sample are shown in Fig. 14(a). The model predictions appear unequivocal up to $z \simeq 3.5$, and one object out of 59 at $z = 3.395$ is well consistent with the range of predictions. The 1-Jy data thus appear to fit well into the framework of the RLFs proposed here, despite the quite large differences between the redshift distribution for this sample and the selected regions which were noted by Dunlop *et al.* (1989a).

A recent addition to the data at this flux-density level has been reported by McCarthy *et al.* (1990). They studied 700 sources from the Molonglo catalogue with $S > 0.95$ Jy at 408 MHz, using the criterion of very steep spectrum to pick out candidate objects at the highest redshifts. Their most distant objects to date has $z = 3.13$, and they estimate that roughly 40 objects from their ultra-steep-spectrum subsample may lie at $z > 2$. Comparison with Fig. 14(a) suggests that a largest redshift slightly above 4 would be predicted for this sample, but that $\gtrsim 70$ objects at $z > 2$ would be expected out of 700. The fact that McCarthy *et al.* find fewer than this may indicate the limitations of the ultra-steep-spectrum approach; compact steep-spectrum sources will probably be systematically missing from such a subsample (Peacock & Wall 1982).

4.4.2 *The Leiden–Berkeley Deep Survey (LBDS)*

This sample (Windhorst 1984; Oort *et al.* 1987 and references therein) is at the faint extreme of the flux-density

range we have considered here. It therefore provides a probe of the high-redshift behaviour of the low-luminosity portion of the RLF. Fig. 14(b) shows the range of predicted redshift distributions for this sample. As no high-redshift data at this flux-density level were used in the modelling, it is not surprising that the redshift content is completely unconstrained beyond $z \simeq 1$. A more interesting plot is shown in Fig. 15: this is the predicted redshift distribution according to the simplified models of Section 3.4. Both pure luminosity evolution and luminosity/density evolution give very similar answers, which is perhaps not so surprising since the low-luminosity slope of the RLF is assumed to be the same in both cases. This diagram thus shows us what would be expected if the RLF peaked at $z \simeq 2$ for all low luminosities. Redshift data at high flux densities will be needed to probe the evolution of the RLF break at high redshift.

It is interesting to compare these results with those of Windhorst (1984). At the time of Windhorst's work, identifications of the LBDS were only partly complete. By extrapolating the evolution seen at $z \lesssim 0.5$, Windhorst argued that a downturn in the RLF beyond $z \simeq 1$ was required in order to avoid exceeding the total counts. This conclusion is clearly consistent with some of our models, but does not appear to be required by the data used here. This may be because we have not used the full LBDS identification data available to Windhorst, or it may indicate a sensitivity of Windhorst's argument to exactly how the extrapolation of low-redshift evolution is performed. On the basis of our PLE and LDE models, the highest redshift in the LBDS would be expected to be just over 4. At present, the highest measured redshift for this sample is $z = 2.4$ (Koo 1989), which suggests that Fig. 15 may not in fact be too far away from the truth.

5 CONCLUSIONS

The principal conclusions from our analysis of the high-redshift evolution of the RLF can be summarized as follows.

(i) Modelling of the flat-spectrum RLF shows that, for objects of high radio luminosity, the comoving density of flat-spectrum radio sources (a population dominated by quasars) suffers a gradual redshift 'cut-off', declining by a factor of $\simeq 5$ between $z = 2$ and $z = 4$.

(ii) Modelling of the steep-spectrum RLF reveals, for the first time, evidence for a similar cut-off in the steep-spectrum population (a population dominated by radio galaxies). This steep-spectrum cut-off appears to be less abrupt than its flat-spectrum counterpart. However, both these statements still depend on the accuracy of our redshift estimates for faint galaxies, and so we have identified those future observations which can remove the remaining uncertainty.

(iii) Direct, model-independent confirmation of the above results is provided by banded versions of the $V/V_{\rm max}$ test. All four classes of source – steep/galaxy, steep/quasar, flat/galaxy, flat/quasar – exhibit a density decline at high redshift, thus indicating that the cut-off is not due to problems with classification.

(iv) The evolution of both the steep- and flat-spectrum RLFs is successfully described by a model of pure luminosity evolution, provided a high value of Ω_0 is assumed. An additional, low-power, non-evolving component is required in the steep-spectrum case, but is superfluous for the flat-spectrum RLF. These models display negative luminosity evolution beyond $z \simeq 2$ in order to reproduce the cut-off.

(v) The data can also be successfully described by a luminosity/density evolution model with suppression of total numbers at high redshift; we therefore cannot yet rule out the possibility that *positive* luminosity evolution of the break in the RLF continues at high redshift.

These results would seem to suggest that, at least as far as evolution is concerned, both flat- and steep-spectrum sources behave very similarly. The traditional two-population approach may therefore not in fact be necessary; at least for powerful sources, it may now be sensible to talk about a *single* evolving RLF. Whether this can be taken as evidence in favour of unified beaming models (Orr & Browne 1982) is not so clear. As we have stressed, however, many of these conclusions depend to an unsatisfactory extent on the correctness of the redshift estimates for the remaining faint galaxies lacking spectroscopy. Our conclusions regarding the steep-spectrum cut-off will only become firm if very few objects beyond $z \simeq 3$ remain to be found in the 2.7-GHz samples considered here.

It is interesting to consider some of the possible interpretations of a redshift cut-off. The first question is whether such an effect could simply be an illusion – the result of obscuration at high redshift. The main process which might affect cm-wavelength radio emission is Thomson scattering due to an ionized intergalactic medium (IGM), though Peacock (1985) showed that, even if all the matter in an $\Omega_0 = 1$ universe is considered to be ionized, an optical depth of only $\tau = 0.2$ is achieved by $z \sim 4$. This can only reduce ρ by 0.2 in $\log_{10}(\rho)$, and the effect is even smaller between $z = 2$ and $z = 4$. It is therefore clear that, at radio wavelengths, obscuration cannot possibly account for the observed cut-off. At optical wavelengths, on the other hand, Ostriker & Heisler (1984) and Heisler & Ostriker (1988) demonstrated that obscuration by dust is capable of producing an apparent high-redshift cut-off. They also noted that, if this dust is unevenly distributed (e.g. associated with galaxies), the few visible high-redshift objects could be seen through 'holes', and need not therefore be heavily reddened. If dust obscura-

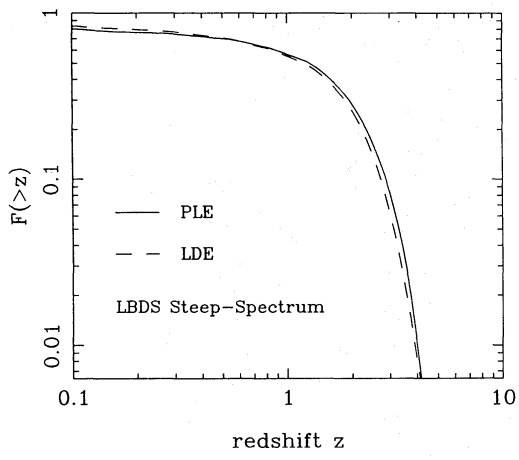

Figure 15. The predicted redshift distributions for the LBDS sample, using the pure luminosity evolution and luminosity/density evolution models of Section 3.4. This suggests that the highest redshifts seen in this sample will be little greater than those found at high flux densities.

tion were in fact a significant effect at optical wavelengths, then a considerable fraction of the selected regions radio sources should have remained unidentified, or at least displayed anomalous optical–infrared colours. The fact that this is not the case gives confidence that studies of optically selected quasars should also not be significantly influenced by obscuration.

It thus seems likely that the redshift cut-off for powerful radio sources is indeed real. It is possible to envisage a variety of models which could give rise to this situation. The evolution of luminosity functions is governed by the conservation equation

$$\dot{\rho}+\frac{\partial}{\partial P}(\dot{P}\rho)=Q, \tag{18}$$

where Q is the rate of source creation. Possibly the most obvious interpretation of the cut-off is to envisage that radio sources were formed during the era $z=2$–4, after which Q fell to zero and sources simply dimmed to the present day. However, the fact that radio sources are known to be short-lived (i.e. $\sim 10^8$ yr) relative to the age of the Universe indicates that $Q\neq 0$ at $z<2$, and also means that one should be careful in interpreting the success of the pure luminosity-evolution model in Section 3.4. The shortness of the lifetimes of radio sources has often led to the interpretation that the evolution of the RLF simply reflects the time variation of the source birth rate – i.e. Q rises from $z=4$ to a peak at $z=2$. Alternatively, Q could in fact be constant, provided $\partial P/\partial t$ increases between $z=2$ and $z=4$; the redshift cut-off might then be the consequence of sources having shorter lifetimes at high redshift.

A complicating factor is the evolution of environment with redshift. Compton snuffing by the microwave background (MWB) has been cited as a possible cause of a high-redshift cut-off, since the energy density of the MWB increases as $(1+z)^4$ (e.g. Rees & Setti 1968), but this mechanism can only affect extended sources, and can thus be discounted since the cut-off is observed for both extended and compact sources. The effect of the IGM is a more difficult problem. Indeed, without detailed information on the cluster environments of the sources in question, it is difficult to decide whether the relevant IGM density increases or decreases with redshift. Various authors (e.g. Eales 1985 and Kapahi, Kulkarni & Subrahmanya 1987) have shown that double radio sources observed at high redshift are smaller than low-redshift sources of the same intrinsic luminosity, and it is interesting to note that most of the (optically) faintest sources in the selected regions are small doubles. It is not clear whether this small size is a consequence of a denser surrounding medium, or whether it simply reflects the youth of the expanding source. Evidence of very distorted radio structures at high redshift (Barthel & Miley 1988; Barthel *et al.* 1988) supports the former explanation. At first sight, increased confinement might be expected to produce more efficient sources by reducing adiabatic losses. However, the opposite result can be envisaged, as indicated by the proposed physical explanation of the difference between FRI and FRII sources (see Prestage & Peacock 1988).

Clearly, therefore, many effects could give rise to a reduction in the comoving density of powerful radio sources at high redshift. It seems plausible, however, that the birth of radio sources (Q) plays an important rôle in producing the observed statistical evolution. This brings us to the fundamental problem of the physical process of radio source formation. There are two classes of explanation to consider: the birth of a radio source may be closely related to the formation of the central black hole, and hence to the formation of the host galaxy. Alternatively it might simply reflect the arrival of a source of fuel (via interaction or merger) which triggers the central engine into action – this may seem more likely to reflect the formation of a cluster. Arguments from stellar populations seem to favour the latter alternative: the high-redshift radio galaxies studied by Lilly (1989) appear to contain stars $\gtrsim 1$ Gyr old, implying formation redshifts $z_f \gtrsim 5$ (see also Dunlop *et al.* 1989b). Theoretical considerations argue against this possibility (see Peacock 1989 for a more detailed discussion). Efstathiou & Rees (1988) have investigated the formation epoch for bound systems in the context of the 'standard' $\Omega_0=1$ cold dark matter model. They find that systems of galactic mass ($\sim 10^{12}\ M_\odot$) should only just be assembled in reasonable numbers by $z\simeq 2$–3. Abell clusters are too massive to have formed by that epoch, and so we are led to consider a direct relation between galaxy formation and the redshift cut-off for active galaxies. In CDM and other hierarchical pictures, star formation in small systems happens long before these can cluster together into massive objects, so the stellar ages may not be relevant; the question is really whether the galaxies we see at $z\simeq 2$ are *dynamically* young. The new generation of large telescopes should make it possible to study both the environments and dynamical properties of high-redshift objects in some detail, and so provide a powerful test of these ideas.

ACKNOWLEDGMENTS

JSD acknowledges financial support from the Royal Society of Edinburgh through the Robert Cormack bequest studentship.

REFERENCES

Allington-Smith, J. R., 1984. *Mon. Not. R. astr. Soc.*, **209,** 665.
Avni, Y. & Bahcall, J. N., 1980. *Astrophys. J.*, **235,** 694.
Avni, Y. & Schiller, N., 1983. *Astrophys. J.*, **267,** 1.
Barthel, P. D. & Miley, G. K., 1988. *Nature,* **333,** 319.
Barthel, P. D., Miley, G. K., Schilizzi, R. T. & Lonsdale, C. J., 1988. *Astr. Astrophys. Suppl.*, **73,** 515.
Bennett, C. L., Lawrence, C. R. & Burke, B. F., 1985. *Astrophys. J.*, **299,** 373.
Boyle, B. J., Shanks, T. & Peterson, B. A., 1988. *Mon. Not. R. astr. Soc.*, **235,** 935.
Boyle, B. J., Fong, R., Shanks, T. & Peterson, B. A., 1987. *Mon. Not. R. astr. Soc.*, **227,** 717.
Cameron, M. J., 1971. *Mon. Not. R. astr. Soc.*, **152,** 429.
Condon, J. J., 1984. *Astrophys. J.*, **287,** 461.
Condon, J. J. & Ledden, J. E., 1982. *Astr. J.*, **87,** 219.
Downes, A. J. B., Peacock, J. A., Savage, A. & Currier, D. R., 1986. *Mon. Not. R. astr. Soc.*, **218,** 31.
Dunlop, J. S., Peacock, J. A., Savage, A., Lilly, S. J., Heasley, J. N. & Simon, A. J. B., 1989a. *Mon. Not. R. astr. Soc.*, **238,** 1171.
Dunlop, J. S., Guiderdoni, B., Rocca-Volmerange, B., Peacock, J. A. & Longair, M. S., 1989b. *Mon. Not. R. astr. Soc.*, **240,** 257.
Eales, S. A., 1985. *Mon. Not. R. astr. Soc.*, **217,** 179.
Efstathiou, G. & Rees, M. J., 1988. *Mon. Not. R. astr. Soc.*, **230,** 5P.

Heisler, J. & Ostriker, J. P., 1988. *Astrophys. J.*, **332,** 543.
Kapahi, V. K., Kulkarni, V. K. & Subrahmanya, C. R., 1987. *J. Astrophys. Astr.*, **8,** 33.
Kellermann, K. I. & Wall, J. V., 1987. In: *Observational Cosmology, IAU Symp. No. 124,* p. 545, eds Hewitt, A., Burbidge, G. & Fang, L. Z., Reidel, Dordrecht.
Koo, D. C., 1986. In: *The Structure and Evolution of Active Galactic Nuclei,* p. 317, eds Giuricin, G., Mardirossian, F., Mezzetti, M. & Ramella, M., Reidel, Dordrecht.
Koo, D. C., 1989. *The Epoch of Galaxy Formation,* p. 71, eds Frenk, C. S., Ellis, R. S., Shanks, T., Heavens, A. F. & Peacock, J. A., NATO ASI C **264,** Kluwer, Dordrecht.
Lilly, S. J., 1988. *Astrophys. J.*, **333,** 161.
Lilly, S. J., 1989. *Astrophys. J.*, **340,** 77.
Lilly, S. J. & Longair, M. S., 1984. *Mon. Not. R. astr. Soc.*, **211,** 833.
Lilly, S. J., Longair, M. S. & Allington-Smith, J. R., 1985. *Mon. Not. R. astr. Soc.*, **215,** 37.
Longair, M. S., 1978. In: *Observational Cosmology,* Saas-Fee Summer School, p. 230, Geneva Observatory, Switzerland.
McCarthy, P. J., Kapahi, V. K., van Breugel, W. & Subrahmanya, C. R., 1990. *High Redshift Radio Galaxies from the Molonglo Catalogue,* Preprint.
Marshall, H. L., 1987. *Astr. J.*, **94,** 628.
Oort, M. J. A., Katgert, P., Steeman, F. W. M. & Windhorst, R. A., 1987. *Astr. Astrophys.*, **179,** 41.
Orr, M. J. L. & Browne, I. W. A., 1982. *Mon. Not. R. astr. Soc.*, **200,** 1067.
Osmer, P. S., 1982. *Astrophys. J.*, **253,** 28.
Osmer, P. S. & Smith, M. G., 1980. *Astrophys. J. Suppl.*, **42,** 333.
Ostriker, J. P. & Heisler, J., 1984. *Astrophys. J.*, **278,** 1.
Peacock, J. A., 1983. *Mon. Not. R. astr. Soc.*, **202,** 615.
Peacock, J. A., 1985. *Mon. Not. R. astr. Soc.*, **217,** 601.
Peacock, J. A., 1989. *The Epoch of Galaxy Formation,* p. 391, eds Frenk, C. S., Ellis, R. S., Shanks, T., Heavens, A. F. & Peacock, J. A., NATO ASI **264,** Kluwer, Dordrecht.
Peacock, J. A. & Gull, S. F., 1981. *Mon. Not. R. astr. Soc.*, **196,** 611.
Peacock, J. A. & Wall, J. V., 1981. *Mon. Not. R. astr. Soc.*, **194,** 331.
Peacock, J. A. & Wall, J. V., 1982. *Mon. Not. R. astr. Soc.*, **198,** 843.
Peacock, J. A., Perryman, M. A. C., Longair, M. S., Gunn, J. E. & Westphal, J. A., 1981. *Mon. Not. R. astr. Soc.*, **194,** 601.
Prestage, R. M. & Peacock, J. A., 1988. *Mon. Not. R. astr. Soc.*, **230,** 131 (erratum: **236,** 959).
Rees, M. J. & Setti, G., 1968. *Nature,* **219,** 127.
Robertson, J. G., 1978. *Mon. Not. R. astr. Soc.*, **182,** 617.
Robertson, J. G., 1980. *Mon. Not. R. astr. Soc.*, **190,** 143.
Rowan-Robinson, M. M., 1968. *Mon. Not. R. astr. Soc.*, **138,** 445.
Sandage, A., 1972. *Astrophys. J.*, **178,** 25.
Savage, A. & Peterson, B. A., 1983. In: *Early Evolution of the Universe and its Present Structure, IAU Symp. No. 104,* p. 57, eds Abell, G. O. & Chincarini, G., Reidel, Dordrecht.
Schmidt, M., 1968. *Astrophys. J.*, **151,** 393.
Schmidt, M., Schneider, D. P. & Gunn, J. E., 1988. In *Proceedings of a workshop on optical surveys for quasars,* eds Osmer, P. S., Porter, A. C., Green, R. F. & Foltz, C. B., *Astr. Soc. Pacif.* Conf. Ser., **2,** 87.
Shanks, T., Fong, R., Boyle, B. J. & Peterson, B. A., 1986. In: *Quasars, IAU Symp. No. 119,* p. 37, eds Swarup, G. & Kapahi, V. K., Reidel, Dordrecht.
Smith, M. G., 1986. In: *Quasars, IAU Symp. No. 119,* p. 17, eds Swarup, G. & Kapahi, V. K., Reidel, Dordrecht.
Subrahmanya, C. R. & Harnett, J. I., 1987. *Mon. Not. R. astr. Soc.*, **225,** 297.
Toffolatti, L., Franceschini, A., De Zotti, G. & Danese, L., 1987. *Astr. Astrophys.*, **184,** 7.
Wall, J. V. & Peacock, J. A., 1985. *Mon. Not. R. astr. Soc.*, **216,** 173.
Wall, J. V., Shimmins, A. J. & Merkelijn, K. J., 1971. *Aust. H. Phys. Astrophys. Suppl.*, **19,** 1.
Wall, J. V., Pearson, T. J. & Longair, M. S., 1980. *Mon. Not. R. astr. Soc.*, **193,** 683.
Wall, J. V., Pearson, T. J. & Longair, M. S., 1981. *Mon. Not. R. astr. Soc.*, **196,** 597.
Wampler, E. J., Robinson, L. B., Baldwin, J. A. & Burbidge, E. M., 1973. *Nature,* **243,** 336.
Warren, S. J., Hewett, P. C. & Osmer, P. S., 1988. In: *Proceedings of a workshop on optical surveys for quasars,* eds Osmer, P. S., Porter, A. C., Green, R. F. & Foltz, C. B., *Astr. Soc. Pacif.* Conf. Ser., **2,** 96.
Wills, D. & Lynds, R., 1978. *Astrophys. J. Suppl.*, **36,** 317.
Windhorst, R. A., 1984. *PhD thesis,* University of Leiden.
Wright, A. E., Jauncey, D. L., Bolton, J. G. & Savage, A., 1982. *Aust. J. Phys.*, **35,** 177.
Yates, M. G., Miller, L. & Peacock, J. A., 1986. *Mon. Not. R. astr. Soc.*, **221,** 311.

APPENDIX A: COMPLETENESS OF THE PARKES SELECTED REGIONS

This appendix considers the internal evidence in the Parkes selected regions for possible incompleteness near the sample limit. We can set some constraints on this through the description of the original survey procedure by Wall, Shimmins & Merkelijn (1971). This consisted of a preliminary finding survey made with an effective receiver noise of 20 mJy, from which candidate objects having $S > 60$ mJy were selected (i.e. a 3σ cut). These objects were then re-observed on long integrations to determine 'true' flux densities. The published list includes all objects where these accurate measurements gave a result greater than the original threshold (approximately 70 per cent of an original list of about 400 candidates). From this information we can readily calculate the expected distribution of flux densities in the final sample; we just need the probability that an object of true flux density S_0 lies above the initial threshold when the initial measuring error is applied. The modified number counts after the finding survey are then

$$\frac{dn'}{dS}(S_0) = \frac{dn}{dS}(S_0) \int_{S_{\rm lim}}^{\infty} p(S|S_0)\, dS.$$

For Gaussian noise, the integral is related simply to the error function. Integrating over these modified number counts from 0 to ∞ and from $S_{\rm lim}$ to ∞ then gives the fraction remaining after re-observation. To carry out this calculation, we need the form of the unperturbed number counts; for simplicity a power law $N(>S) \propto S^{-1.3}$ was adopted (with a normalization fixed by the numbers above 0.2 Jy). Reasonable variations about this form make little difference to the answer.

Fig. A1 shows the histogram of flux densities in the selected regions after re-observation, together with the above prediction. The agreement is poor, with too few objects by a factor of ~ 2 at $S \lesssim 0.1$ Jy. The simplest conjecture about what has gone wrong is that the original finding survey was not complete to the stated limit of 0.06 Jy: something closer to 0.08 Jy would give about the right number of objects in 0.06 Jy $\lesssim S \lesssim$ 0.1 Jy. However, this would predict a fraction of objects lying below 0.06 Jy after remeasuring which is very much smaller than the observed 30 per cent. We can model this number and the distribution of remeasured flux densities successfully only by assuming that neither the noise nor the limit of the finding survey were as stated. A noise of 0.03 Jy and a finding limit of 0.07 Jy are consistent with the

available information; this curve is also shown on Fig. A1. On this basis, the incompleteness at 0.1 Jy would be a factor of about 1.25.

These calculations confirm that there is a problem from internal evidence alone, but do not tell us what it is. The best estimate of the incompleteness is probably that derived from the comparison with other count data in Section 2.2. There is evidence for a large deficit only in the steep-spectrum data, which seems bizarre, but there is apparently no way in which a spectrum-dependent bias could be introduced (at this flux-density level, the median angular size is only a few arcsec and so resolution effects from the 8-arcmin Parkes beam should be negligible). On this basis, a correction of total numbers in the 100–120 μJy bin by a factor of about 1.5 is suggested (higher factors are ruled out by the flat-spectrum counts, lower factors by the steep-spectrum data). Such a correction would be consistent with the above internal analysis.

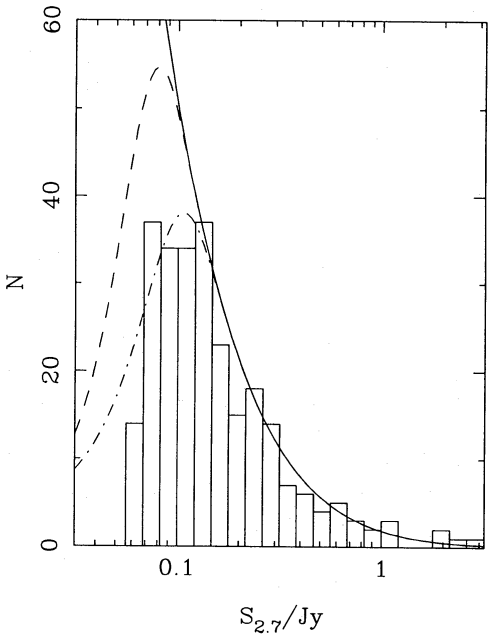

Figure A1. The flux-density histogram of all objects from the Parkes selected regions finding survey which had $S > 0.06$ Jy after remeasuring. The solid line is a model for the unperturbed number counts: $N(>S) \propto S^{-1.3}$. The dashed line shows the predicted flux-density distribution according to the parameters given for the finding survey: $S_{\rm lim} = 0.06$ Jy and a noise of 0.02 Jy. The dot-dashed line shows the distribution expected if in reality these parameters were $S_{\rm lim} = 0.07$ Jy and the noise 0.03 Jy.

APPENDIX B: CANDIDATE ULTRA-HIGH-REDSHIFT OBJECTS

To focus attention on those objects in the complete data sets we have used which may lie at very large redshifts, we list below those objects for which the possibility of $z \gtrsim 2$ exists. We therefore exclude objects with a spectroscopic redshift, and also those for which the identification is definitely a galaxy which satisfies certain criteria on brightness: if any one of the conditions $K < 17.5$, $(B, V, R) < 21$ is satisfied, we take it as being essentially certain that the object in question lies at $z < 2$. This leaves a total of 72 out of 352 steep-spectrum sources (20 per cent) and 31 out of 171 flat-spectrum sources (18 per cent). If, as seems probable, all the G? objects do turn out to be galaxies, this would remove a further 31 objects from consideration, leaving in total 72 out of 523 sources (14 per cent).

Obtaining spectroscopy for these objects is clearly a very high priority. At present, there are a total of 27 objects with spectroscopic $z > 2$ and a further 25 in the above lists are estimated to lie at $z \geq 2$. It is therefore a theoretical possibility that the bulk of radio sources in these samples which lie

Table B1. Steep-spectrum sources from the bright 2.7-GHz samples.

(1) IAU	(2) Name	(3) α (1950)	(4) δ (1950)	(5) $S_{2.7}$	(6) $\alpha^5_{2.7}$	(7) ID	(8) V	(9) z_{est}	(10) refs
0008−42		00 08 21.30	−42 09 50.6	2.47	1.03	EF		1.6	8, 1
0022−42		00 22 15.42	−42 18 40.7	2.84	0.77	G?	20.6	0.7	1
0114−21	OC−224	01 14 25.95	−21 07 55.0	2.23	0.95	EF		1.6	4
0117−15	3C38	01 17 59.74	−15 36 00.7	2.72	0.90	G?	21.0	0.8	4
0223+34	4C34.07	02 23 09.75	34 07 59.9	1.80	0.53	G?	22.0	1.3	3
0235−19	OD−159	02 35 24.77	−19 45 31.7	2.41	0.87	G?	20.3	0.6	4
0316+16	CTA21	03 16 09.11	16 17 41.4	4.77	0.79	G	22.7	1.7	16, 15
0404+76	4C76.03	04 04 01.06	76 48 52.7	4.05	0.60	G	21.7	1.1	3
0407+74	4C74.08	04 07 03.98	74 43 32.2	1.69	0.90	G?	20.0	0.5	14
0409−75		04 09 58.94	−75 14 57.1	7.23	0.86	G?	21.5	1.0	1
0825−20	OJ−242	08 25 03.40	−20 16 31.0	2.10	0.94	Q	18.0	0.9	9
0834−19	OJ−158.1	08 34 56.36	−19 41 14.5	2.50	0.82	G?	20.3	0.6	15
1015−31	OL−327	10 15 53.38	−31 29 11.7	2.22	0.84	G?	20.2	0.6	4
1225+36	ON343	12 25 30.90	36 51 48.6	1.60	1.17	G?	22.4	1.5	3
1245−19	ON−176.2	12 45 45.24	−19 42 58.2	3.94	0.76	G?	19.5	0.4	10
1306−09	OP−10	13 06 02.01	−09 34 31.8	2.80	0.65	G?	20.5	0.6	4
1308−22	3C283	13 08 57.40	−22 00 46.7	2.43	1.30	G?	21.5	1.0	1
1413+34	OQ323	14 13 56.29	34 58 29.5	1.72	0.60	G?	22.7	1.7	3
1518+04	4C04.51	15 18 44.73	04 41 05.5	2.20	1.28	G?	22.8	1.8	1
1607+26	CTD93	16 07 09.29	26 49 18.6	3.04	1.08	G?	21.0	0.8	1
1733−56		17 33 21.43	−56 32 16.0	5.20	0.73	G?	17.0	0.1	17, 18
1819+39	4C39.56	18 19 42.26	39 41 15.4	1.80	0.98	G?	19.0	0.3	7
1829+29	4C29.56	18 29 17.89	29 04 58.3	1.91	0.80	G?	20.5	0.6	14
1938−15	OV−164	19 38 24.80	−15 31 34.0	3.80	0.82	G?	21.5	1.0	1
2008−06	OW−15	20 08 33.66	−06 53 00.9	2.20	0.82	G	21.8	1.1	15
2032−35	OW−354	20 32 37.08	−35 04 29.7	3.70	1.10	G?	21.5	1.0	1
2150−52		21 50 48.17	−52 04 23.9	2.10	0.95	G?	22.2	1.4	1

Table B2. Flat-spectrum sources from the bright 2.7-GHz samples.

(1)	(2)	(3)	(4)	(5)	(6)	(7)	(8)	(9)	(10)
IAU	Name	α (1950)	δ (1950)	$S_{2.7}$	$\alpha_{2.7}^{5}$	ID	V	z_{est}	refs
0115−01	4C−1.07	01 15 42.27	−01 36 14.9	0.64	0.22	G?	21.0	0.8	2, 1
0202+14	4C15.05	02 02 07.43	14 59 52.0	3.00	0.43	G?	22.6	1.7	3
0213−02	4C−2.09	02 13 09.84	−02 36 49.9	0.54	−0.58	G?	19.1	0.3	2, 1
0422+00		04 22 12.48	00 29 17.8	1.28	−0.36	Q	16.3	0.4	2
0500+01	OG3	05 00 45.18	01 58 53.8	2.47	0.47	G?	21.4	1.0	1
0742+10	OI471	07 42 48.47	10 18 32.6	3.74	0.08	G?	23.6	2.6	15
0814+42	OJ425	08 14 51.68	42 32 07.5	2.24	0.47	Q	17.7	0.7	3
0823+03		08 23 13.56	03 19 15.7	1.03	0.15	Q?	17.5	0.7	2
0837+03		08 37 12.37	03 30 33.1	0.69	0.28	Q?	20.5	3.3	2
0945+66	4C66.09	09 45 15.02	66 28 59.0	1.64	0.46	G	22.3	1.4	3
1317+01		13 17 53.80	01 56 19.0	0.59	0.00	G?	20.4	0.6	2
1538+14	4C14.60	15 38 30.21	14 57 21.4	1.98	0.01	Q?	15.5	0.4	13, 12
1622−25	OS−237.8	16 22 44.11	−25 20 51.5	2.27	0.19	G?	21.9	1.2	8, 1
1624+41	4C41.32	16 24 18.25	41 41 23.3	1.60	0.30	G?	23.1	2.1	15
2012−01		20 12 39.74	−01 46 44.9	0.78	0.35	Q	17.2	0.6	2
2047+03		20 47 36.03	03 56 35.0	0.57	−0.16	Q	22.3	1.4	2
2215+02		22 15 15.56	02 05 08.8	0.65	0.05	G?	21.1	0.8	2, 1
2224+00	4C0.81	22 24 13.08	00 36 53.5	0.52	0.10	G?	21.8	1.1	2, 1
2245+02		22 45 25.96	02 54 51.9	0.73	0.29	Q?	20.1	2.6	2
2324+40	3C462	23 24 30.54	40 31 37.1	1.53	0.48	G?	18.9	0.3	11
2351+45	4C45.51	23 51 49.76	45 36 22.4	1.50	0.08	G?	20.6	0.7	11

Table B3. Steep-spectrum sources from the Parkes selected regions.

(1)	(2)	(3)	(4)	(5)	(6)	(7)	(8)	(9)	(10)	(11)
IAU	α (1950)	δ (1950)	$S_{2.7}$	$\alpha_{2.7}^{1.4}$	Structure	ID	B	R	K	z_{est}
0000+035	00 00 37.68	03 33 36.4	0.146	1.41	P	G?	23.01	21.27		0.8
0043−010	00 43 33.14	−01 00 04.7	0.188	0.82	P	G	>23.00	23.04	17.64	1.6
0043−003	00 43 56.99	−00 21 54.1	0.100	1.07	Do,II	G?	>23.50	>23.00	18.30	2.3
0051−008	00 51 49.34	−00 49 30.2	0.137	0.82	Do,II	G?	>23.00	22.48	17.20	1.3
0059+017	00 59 41.11	01 47 01.5	0.400	1.06	Do,II	G?	23.41	21.36		0.6
0105+034	01 05 49.93	03 25 34.1	0.181	0.64	U	?	24.18		18.59	2.8
0105+025	01 05 50.09	02 33 50.0	0.122	0.87	Do,II/D2?	G?	>24.00	>23.50	17.26	1.3
0223−023	02 23 02.10	−02 23 47.8	0.225	0.93	P	G?	>23.50	22.61	17.32	1.3
0223+035	02 23 19.48	03 33 51.3	0.142	1.09	Do,II	G?	23.30	22.45	17.55	1.5
0225+002	02 25 31.94	00 17 54.4	0.141	1.15	Do,II	G?	>24.00	>24.00	18.54	2.7
0227+001	02 27 04.19	00 11 56.2	0.131	1.15	Do+CC,II	?	23.16		17.98	2.0
0238−018	02 38 21.67	−01 50 57.8	0.102	1.19	Do,II	Q	19.10	19.60	16.29	1.0
0245+013	02 45 12.62	01 18 54.2	0.153	1.01	Do,II	G	23.84	23.96	18.01	2.0
1159−023	11 59 58.51	−02 23 21.4	0.430	1.03	P	G?	>24.00	>23.50	18.30	2.3
1201−026	12 01 08.27	−02 38 27.2	0.143	1.07	Do,II	G?	23.11	22.87	18.17	2.2
1212−007	12 12 14.96	−00 43 35.7	0.510	1.00	Do,II	G?	23.25		17.87	1.8
1214−029	12 14 31.97	−02 54 57.0	(0.131)	1.06	HT,I	?	22.07	21.05		1.2
1331+004	13 31 07.24	00 26 21.5	0.140	1.44	Do,II	G?	23.14	22.06	17.81	1.8
1336+003	13 36 07.50	00 18 00.6	0.117	1.05	Do+CC,II	G?	24.09	23.13	18.60	2.8
1337−033	13 37 37.96	−03 20 09.2	0.580	0.84	U	G?	22.90	21.68	17.70	1.7
1339+015	13 39 44.04	01 32 24.1	0.172	0.86	U	?	24.97	24.09	18.00	2.0
1345+008	13 45 06.70	00 49 54.2	0.139	1.21	Do,II	G?	24.23	23.70	18.20	2.2
1349−019	13 49 22.98	−01 55 10.6	0.139	1.11	Do,II	G?	>24.00	>24.00	17.90	1.9
1349−008	13 49 52.53	−00 52 49.3	0.137	0.93	Do,II	G	23.31	22.02		1.0
1352+008	13 52 34.20	00 55 24.9	0.400	0.85	U	G?	23.77	22.64	17.00	1.1
2150−202	21 50 56.15	−20 15 19.0	0.310	0.95	Do,II	G?	22.96	22.45		1.7
2157−214	21 57 10.08	−21 25 05.6	0.167	0.96	Do,II	?	21.20	20.51	16.79	1.0
2157−191	21 57 55.75	−19 10 06.6	0.133	0.97	Do,II	G	23.78	22.71	17.63	1.6
2158−170	21 58 53.13	−17 03 02.0	0.178	1.12	D2	G?	>24.50	>24.00	18.44	2.5
2159−215	21 59 03.34	−21 32 34.0	0.130	1.15	P	G	23.50	22.25	18.21	2.2
2159−192	21 59 27.27	−19 17 21.3	0.169	1.07	Do,II	G	24.21	23.34	17.94	1.9
2159−201	21 59 56.05	−20 09 40.3	0.200	1.66	Do,II/D2?	G?	>24.50	23.20		1.0
2200−189	22 00 06.80	−18 54 24.7	0.167	0.68	U	?	>23.00	22.07	18.55	2.7
2202−179	22 02 14.50	−17 57 08.7	0.340	1.11	Do,II	G?	21.84	20.89	16.79	1.0
2204−182	22 04 11.88	−18 15 27.2	0.340	0.83	Do,II	G?	>24.00	23.82	>19.00	3.5
2205−178	22 05 21.48	−17 52 11.8	0.152	1.21	Do+CC,II	?	23.63	22.30	>19.00	3.5
2213−156	22 13 51.94	−15 39 11.1	0.281	0.80	Do+CC,II	?	21.20	21.22	17.03	1.1
2215−185	22 15 37.47	−18 35 04.7	0.104	1.10	Do,II	G?	>23.50	23.01		1.7
2355−024	23 55 27.29	−02 27 26.6	0.151	0.80	P,V	Q?	22.93	22.37	>19.00	3.5
2356+018	23 56 41.94	01 50 13.1	0.156	0.85	Do,II	G?	20.80	19.59	16.14	0.7
2357−006	23 57 27.97	−00 38 52.2	0.147	0.66	P	G?	>24.00	>23.50	17.97	2.0

Table B4. Flat-spectrum sources from the Parkes selected regions.

(1)	(2)	(3)	(4)	(5)	(6)	(7)	(8)	(9)	(10)	(11)
IAU	α (1950)	δ (1950)	$S_{2.7}$	$\alpha_{2.7}^{1.4}$	Structure	ID	B	R	K	z_{est}
0005+021	00 05 10.05	02 09 49.7	0.117	0.36	U,V	Q?	24.40	>23.00		1.0
0008−006	00 08 18.77	−00 36 47.8	0.106	0.43	U,V	Q?	23.95	22.88	18.94	3.3
0017+026	00 17 12.41	02 41 29.2	0.142	0.00	U,V	G?		21.99	16.72	0.9
0047+023	00 47 08.88	02 20 44.3	0.319	0.23	U,V	Q	19.00	18.20?	17.78	1.7
0223+018	02 23 39.86	01 51 48.2	0.220	0.45	Do,II	Q?	21.68	21.11		1.6
0241−012	02 41 16.57	−01 15 42.5	0.107	0.26	Do,II	G?	>23.50	23.58	17.15	1.2
1157+026	11 57 01.59	02 36 49.5	0.133	0.23	U	G?	24.05	>23.50	17.20	1.3
1205+011	12 05 59.94	01 11 03.8	0.231	−0.18	U	G?	23.59?	21.64	17.20	1.3
2158−167	21 58 11.07	−16 46 59.5	0.147	0.12	Do+CC,I	?	20.70	20.64	16.60	0.9
2354−021	23 54 51.31	−02 08 57.4	0.287	0.07	P,V	Q?	21.16	20.20	15.81	3.6

at $z>2$ have not yet been identified spectroscopically. We have tried to argue that this is unlikely, but clearly proof will be required. We hope that these tables will encourage spectroscopists to go out and attempt to verify our redshift estimates.

The tables include optical positions where an accurate (subarcsec) measure is available, otherwise radio. We give the estimated redshifts which are used in this paper. Numbered references for the tables are as follows.

1. Our unpublished data. Peacock, Prestage & Wall, in preparation.

2. McEwan, N. J., Browne, I. W. A. & Crowther, J. H., 1975. *Mem. R. astr. Soc.*, **80,** 1.

3. Peacock, J. A., Perryman, M. A. C., Longair, M. S., Gunn, J. E. & Westphal, J. A., 1981. *Mon. Not. R. astr. Soc.*, **194,** 601.

4. Prestage, R. M. & Peacock, J. A., 1983. *Mon. Not. R. astr. Soc.*, **204,** 355.

5. Biretta, J. A., Schneider, D. P. & Gunn, J. E., 1985. *Astr. J.*, **90,** 2508.

6. Bolton, J. G., Clark, M. E. & Ekers, R. D., 1965. *Aust. J. Phys.*, **18,** 627.

7. Véron, M. P., Véron, P., Adgie, R. L. & Gent, H., 1976. *Astr. Astrophys.*, **47,** 401.

8. Perley, R. A., 1982. *Astr. J.*, **87,** 859.

9. Bolton, J. G. & Kinman, T. D., 1966. *Astrophys. J.*, **145,** 951.

10. Walter, H. G. & West, R. M., 1980. *Astr. Astrophys.*, **86,** 1.

11. Cohen, A. M., Porcas, R. W., Browne, I. W. A., Daintree, E. J. & Walsh, D., 1979. *Mem. R. astr. Soc.*, **84,** 1.

12. Wills, B. J., 1976. *Astr. J.*, **81,** 1031.

13. Véron, M. P., 1971. *Astr. Astrophys.*, **11,** 1.

14. Kühr, H., 1980. *PhD thesis,* University of Bonn.

15. Fugmann, W., Meisenheimer, K. & Röser, H.-J., 1988. *Astr. Astrophys. Suppl.*, **75,** 173.

16. Allen, D. A., Wright, A. E. & Ables, J. G., 1982. *J. Astrophys. Astr.*, **3,** 189.

17. Lü, P. K., 1970. *Astr. J.*, **75,** 1164.

18. Christiansen, W. N., Frater, R. H., Watkinson, A., O'Sullivan, J. D., Lockhart, I. A. & Goss, W. M., 1977. *Mon. Not. R. astr. Soc.*, **181,** 183.

APPENDIX C: THE RLF EXPANSION COEFFICIENTS

This appendix gives the expansion coefficients of the model radio luminosity functions described in Section 3. Table C1 gives the expansion coefficients for the five free-form models in the ensemble which were derived using the data involving the MEAN-z estimated redshifts for faint galaxies. Table C2 gives the corresponding coefficients for the free-form model ensemble based on the HIGH-z data set. Tables C3 and C4 give parameters for the luminosity and luminosity/density evolution models, respectively.

Table C1. RLF expansion coefficients for models 1–5, MEAN-z data.

order of term		Steep-spectrum				
x	y	RLF1	RLF2	RLF3	RLF4	RLF5
0	0	−2.50	−2.54	−2.46	−2.46	−2.49
1	0	−6.87	−6.58	−6.69	−6.31	−6.36
0	1	9.58	10.83	−3.76	3.73	3.78
2	0	−19.19	−12.76	−21.80	−24.00	−23.05
1	1	92.02	114.64	−10.67	57.48	45.88
0	2	73.77	−52.05	163.29	300.43	342.11
3	0	17.34	−50.25	39.72	27.44	23.13
2	1	−825.22	−1260.32	−117.55	−363.60	−370.21
1	2	607.98	1765.47	28.13	−425.41	−424.52
0	3	−1394.94	−1259.21	−686.19	−2754.74	−2837.02
4	0	161.87	417.02	89.94	148.81	162.15
3	1	2071.14	3486.80	559.09	621.32	732.23
2	2	−2817.94	−7066.62	−1715.58	887.24	646.76
1	3	3826.04	6715.16	3486.97	4180.83	3980.09
0	4	471.47	−1363.82	−1048.00	1290.92	1991.58
5	0	−427.37	−851.72	−313.07	−383.71	−406.20
4	1	−1477.14	−2687.25	−456.48	−85.26	−211.06
3	2	2423.76	6495.46	2004.55	−2439.16	−2097.36
2	3	−2778.27	−7112.88	−4095.20	2376.92	2413.01
1	4	−250.68	2240.36	2240.40	−4200.29	−4625.92
0	5	−198.64	−133.62	−354.41	−91.32	−267.79
6	0	276.73	532.10	193.89	219.42	234.36

order of term		Flat-spectrum				
x	y	RLF1	RLF2	RLF3	RLF4	RLF5
0	0	−3.68	−3.65	−3.74	−3.68	−3.87
1	0	−9.19	−9.85	−8.65	−9.46	−7.42
0	1	−1.84	−2.68	0.25	−1.77	21.39
2	0	6.77	7.87	6.66	7.93	−2.57
1	1	60.41	113.69	−3.85	67.82	−51.09
0	2	−222.49	−327.29	−4.93	−257.06	−129.69
3	0	−17.47	−15.87	−20.83	−20.25	2.47
2	1	49.99	−102.75	76.34	80.36	229.88
1	2	51.87	273.76	−28.32	−150.46	−293.03
0	3	451.96	644.35	−2.33	915.03	609.15
4	0	3.48	0.99	8.10	5.68	−9.94
3	1	−87.58	25.99	−87.30	−136.31	−182.70
2	2	51.88	−74.47	85.66	316.68	304.14
1	3	−215.62	−405.87	−67.13	−576.82	−249.17
0	4	−198.28	−293.40	28.07	−506.21	−389.71

Table C2. RLF expansion coefficients for models 1–5, HIGH-z data.

order of term		Steep-spectrum				
x	y	RLF1	RLF2	RLF3	RLF4	RLF5
0	0	−2.47	−2.52	−2.44	−2.56	−2.52
1	0	−7.15	−6.41	−6.74	−6.11	−6.26
0	1	6.76	6.93	−1.22	12.37	6.19
2	0	−20.77	−18.49	−19.22	−19.14	−23.20
1	1	96.04	86.23	2.36	34.72	32.06
0	2	139.94	154.94	91.96	52.94	340.91
3	0	35.83	−7.29	17.14	−1.04	24.97
2	1	−796.17	−776.20	−167.41	−359.39	−376.25
1	2	318.77	144.15	71.48	444.25	−413.74
0	3	−1512.51	−1206.15	−372.90	−1778.76	−2742.14
4	0	106.72	269.68	154.13	213.32	158.03
3	1	2010.00	2066.78	602.62	605.48	758.34
2	2	−2446.57	−2357.30	−1204.05	35.65	694.75
1	3	4157.98	3930.41	1946.45	839.07	4022.71
0	4	512.03	166.80	−553.65	2650.38	1911.39
5	0	−361.94	−615.89	−397.27	−449.54	−401.07
4	1	−1449.15	−1550.84	−479.68	−46.91	−185.13
3	2	2283.74	2462.66	1394.17	−2205.02	−2260.05
2	3	−2983.41	−3158.13	−2399.76	5066.31	2191.75
1	4	−339.03	−33.70	1270.06	−6645.97	−4506.29
0	5	−189.67	−114.80	−205.09	964.72	−19.45
6	0	249.92	393.91	241.13	243.60	228.57

order of term		Flat-spectrum				
x	y	RLF1	RLF2	RLF3	RLF4	RLF5
0	0	−3.67	−3.65	−3.74	−3.71	−3.69
1	0	−9.44	−9.86	−8.72	−9.61	−9.32
0	1	−0.99	−3.84	−0.27	−0.73	−0.99
2	0	6.96	9.05	8.89	12.06	7.59
1	1	77.80	105.29	−8.11	36.75	57.34
0	2	−279.85	−284.96	0.03	−216.00	−221.11
3	0	−16.43	−21.12	−29.12	−34.44	−23.07
2	1	9.83	−54.71	101.90	183.18	102.60
1	2	140.12	155.39	−57.31	−200.64	−38.65
0	3	531.99	535.69	3.93	637.75	392.75
4	0	2.23	6.08	15.10	19.60	13.32
3	1	−64.69	−21.40	−108.24	−253.85	−215.76
2	2	18.59	10.46	98.30	510.35	521.19
1	3	−282.09	−289.09	−53.89	−726.70	−961.68
0	4	−227.63	−229.22	20.71	−14.27	493.58

Table C3. Best-fit model parameters for pure luminosity evolution ($\Omega_0 = 1$), MEAN-z data.

parameter	Steep-spectrum	Flat-spectrum
ρ_0	−6.91	−8.15
α	0.69	0.83
β	2.17	1.96
a_0	24.89	25.26
a_1	1.26	1.18
a_2	−0.26	−0.28
b_0	−2.86	
b_1	6.93	
b_2	−10.21	
b_3	−728.28	
b_4	1164.50	
b_5	750.97	
b_6	−1385.71	

Table C4. Best-fit model parameters for luminosity/density evolution ($\Omega_0 = 1$).

	Steep-spectrum		Flat-spectrum	
parameter	MEAN-z	HIGH-z	MEAN-z	HIGH-z
η	1.37	1.44	1.37	1.44
α	0.73	0.70	0.85	0.86
β	2.22	2.20	2.00	2.02
a_0	24.55	24.46	24.73	24.76
a_1	3.17	3.50	3.22	3.30
c_0	−6.62	−6.53	−7.87	−7.89
c_1	−10.97	−12.66	−5.74	−8.79
c_2	97.91	92.35	93.06	127.90
c_3	−338.51	−280.74	−738.92	−794.78
c_4	434.38	370.45	2248.76	1873.03
c_5	−186.92	−178.80	−2399.45	−1484.69
b_0	−3.04	−2.92		
b_1	12.03	8.61		
b_2	−30.72	−15.01		
b_3	−861.88	−774.07		
b_4	1607.06	1236.81		
b_5	416.71	809.68		
b_6	−1365.84	−1475.06		